Accepted Manuscript

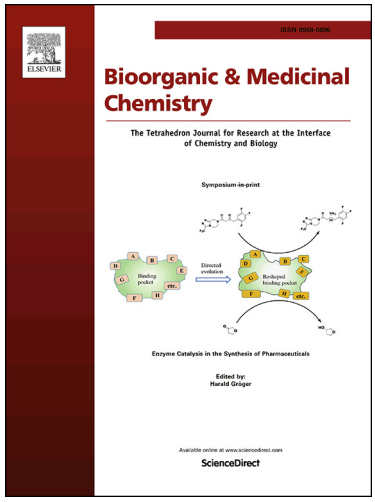

Synthesis, biological evaluation, and molecular docking study of novel allyl-retrochalcones as a new class of protein tyrosine phosphatase 1B inhibitors

Yunjie Zhao, Yongkai Cao, Huizhen Chen, Fei Zhuang, Chao Wu, Goo Yoon, Weiwei Zhu, Ying Su, Suqing Zheng, Zhiguo Liu, Seung Hoon Cheon

PII: S0968-0896(18)32043-1
DOI: https://doi.org/10.1016/j.bmc.2019.01.034
Reference: BMC 14726

To appear in: *Bioorganic & Medicinal Chemistry*

Received Date: 4 December 2018
Revised Date: 26 January 2019
Accepted Date: 29 January 2019

Please cite this article as: Zhao, Y., Cao, Y., Chen, H., Zhuang, F., Wu, C., Yoon, G., Zhu, W., Su, Y., Zheng, S., Liu, Z., Cheon, S.H., Synthesis, biological evaluation, and molecular docking study of novel allyl-retrochalcones as a new class of protein tyrosine phosphatase 1B inhibitors, *Bioorganic & Medicinal Chemistry* (2019), doi: https://doi.org/10.1016/j.bmc.2019.01.034

Synthesis, biological evaluation, and molecular docking study of novel allyl-retrochalcones as a new class of protein tyrosine phosphatase 1B inhibitors

Yunjie Zhao [1,2 #], Yongkai Cao [3,#], Huizhen Chen [4,#], Fei Zhuang [1], Chao Wu [1], Goo Yoon [5], Weiwei Zhu [1], Ying Su [1], Suqing Zheng [1], Zhiguo Liu [1,*], Seung Hoon Cheon [2,*]

[1] Chemical Biology Research Center at School of Pharmaceutical Sciences, Wenzhou Medical University, 1210 University Town, Wenzhou, Zhejiang 325035, China.

[2] College of Pharmacy and Research Institute of Drug Development, Chonnam National University, 77 Yongbong-Ro, Buk-Gu, Gwangju 61186, Korea.

[3] Guangdong Key Laboratory for Genome Stability & Disease Prevention, School of Pharmaceutical Science, Shenzhen University Health Science Center, Shenzhen, 518060, China.

[4] College of Chemistry & Materials Engineering, Wenzhou University, Wenzhou, Zhejiang 325035, China.

[5] College of Pharmacy and Natural Medicine Research Institute, Mokpo National University, Jeonnam 58554, Korea.

[#] These authors contribute equally to this work.

* Corresponding authors:

Zhiguo Liu, Professor

Chemical Biology Research Center at School of Pharmaceutical Sciences, Wenzhou Medical University, 1210 University Town, Wenzhou, Zhejiang 325035, China.

Tel. +8686699892

Fax. +8686699892

Email: lzgcnu@163.com

Seung Hoon Cheon, Professor

College of Pharmacy and Research Institute of Drug Development, Chonnam National University, 300 Yongbong-Dong, Buk-Gu, Gwangju 500-757, Korea.

Tel. +82625302929

Fax. +82625302949

Email: shcheon@jnu.ac.kr

Abstract

We describe herein the design, synthesis, and biological evaluation of a series of novel protein tyrosine phosphatase 1B (PTP1B) inhibitor retrochalcones having an allyl chain at the C-5 position of their B ring. Biological screening results showed that the majority of these compounds exhibited an inhibitory activity against PTP1B. Thus, preliminary structure-activity relationship (SAR) and quantitative SAR analyses were conducted. Among the compounds, **23** was the most potent inhibitor, exhibiting the highest *in vitro* inhibitory activity against PTP1B with an IC_{50} of 0.57 μM. Moreover, it displayed a significant hepatoprotective property via activation of the IR pathway in type 2 diabetic db/db mice. In addition, the results of our docking study showed that **23,** as a specific inhibitor of PTP1B, effectively transformed the WPD loop from "close" to "open" in the active site. These results may reveal suitable compounds for the development of PTP1B inhibitors.

Keywords: Allyl-retrochalcone, Protein tyrosine phosphatase 1B, Drug design, Structure-activity relationship.

1. Introduction

Phosphorylation and dephosphorylation are catalyzed by the coordinated actions of protein kinases and phosphatases, respectively. They are among the most important modifications that modulate protein function in nearly all biological systems to transfer information between distinct cellular sites and to control a wide variety of cellular functions.[1] Although the molecular mechanism of insulin resistance and obesity is not fully understood, the binding of insulin to the insulin receptor induces autophosphorylation of tyrosine residues in its intracellular domain, triggering a kinase cascade.[2] Protein tyrosine phosphatase 1B (PTP1B) has been shown to dephosphorylate the insulin receptor and downregulate insulin signaling. It has been found that decreased phosphorylation of protein tyrosine of the insulin receptor is caused by increased activity of protein tyrosine phosphatase 1B instead of by a lack of tyrosine kinase activity.[3] Consequently, a selective PTP1B

inhibitor will increase the half-life of phosphorylated insulin receptor and maintain the receptor in an activated state.

PTP1B is an attractive target for the treatment of both type 2 diabetes and obesity. Animal studies have shown that PTP1B-deficient mice show enhanced insulin sensitivity, improved glycemic control, and resistance to high fat diet-induced obesity.[4-6] It has also been shown that the downregulation of PTP1B expression by a designed antisense oligonucleotide normalizes blood glucose and improves insulin sensitivity without changing the diet of mice.[7] These results attracted considerable interest in the discovery of small-molecule PTP1B inhibitors to treat type 2 diabetes, which is characterized by insulin resistance and beta-cell dysfunction. The discovery of clinically useful PTP1B inhibitors, although heavily investigated worldwide, has proven to be very difficult because of their limited selectivity and unfavorable pharmacokinetics.[8,9] This difficulty suggests a need to investigate compounds that can overcome these major hurdles in phosphatase inhibitor research.[10] Unlike kinase inhibitors, no phosphatase inhibitor has been approved by the FDA to treat human diseases. Currently, two PTP1B inhibitors are being clinically developed, TTP814 and trodusquemine (MSI-1436), which are currently in Phase II and Phase Ib trials for type 2 diabetes, respectively.[11,12]

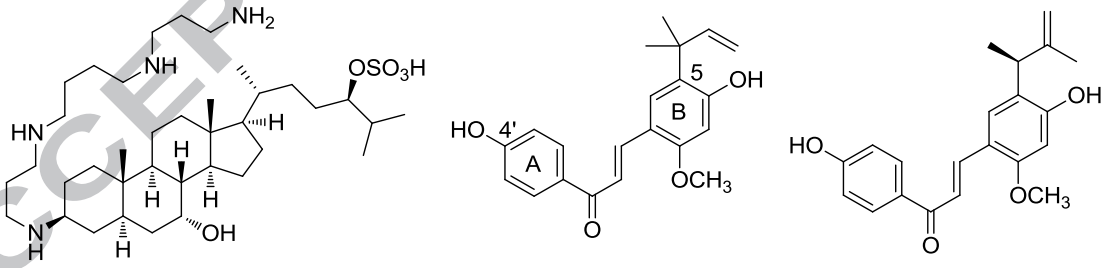

Figure 1. Structures of trodusquemine, licochalcone A, and licochalcone E.

Retrochalcone is an exceptional chemical template having multifarious biological activities.[13-15] In our previous study, which is a further development of our research program, licochalcones A and E (Figure 1), each with an allyl group at position C-5 of the B ring, exhibit significant inhibitory effects against PTP1B. Licochalcone A derivative with methylation at the 4'-hydroxy position exhibit approximately two-fold higher activities than that of licochalcone A.[16] From this finding, we can

conclude that an allyl group at position 5 of retrochalcones is essential in its protective effect against PTP1B activities *in vitro*. Thus, we synthesized analogs of allyl-retrochalcones in order to evaluate changes in bioactivity that result from the varied substituent groups attached to the phenol ring. Interestingly, most of the synthetic allyl-retrochalcone derivatives displayed significant inhibitory effects against PTP1B**.** Herein, we report the design, synthesis, and evaluation of new allyl-retrochalcone derived from licochalcones A and E as PTP1B inhibitors.

2. Chemistry

The synthesis of the allyl-retrochalcone derivatives **1-39** is illustrated in Scheme **1** and **2**. Allylation of the commercially available 4-hydroxy-2-methoxybenzaldehyde **(1a)** with allyl bromide to yield allyl phenyl ether **2a**.[17] Claisen rearrangement of **2a** in boiling *N*,*N*-dimethylaniline solvent afforded allyl-benzaldehyde **3a**, which was further protected with MOMCl/NaH to obtain the benzaldehyde **4a** with an excellent yield. Coupling of **4a** by aldol condensation with commercially available or previously synthesized acetophenones in an ethanolic solution readily generated the protective allyl-retrochalcone **5a**. The final allyl-retrochalcone derivatives, **1**, **3-8**, and **10-30**, were obtained by deprotection of **5a** under acidic conditions. Alternatively, protection of the 4-hydroxy group of **3a** with 3,4-dihydro-2*H*-pyran in THF generated Compound **6a,** which was further coupled with corresponding acetophenones to obtain Compounds **2** and **9** with catalyzation by KOH.

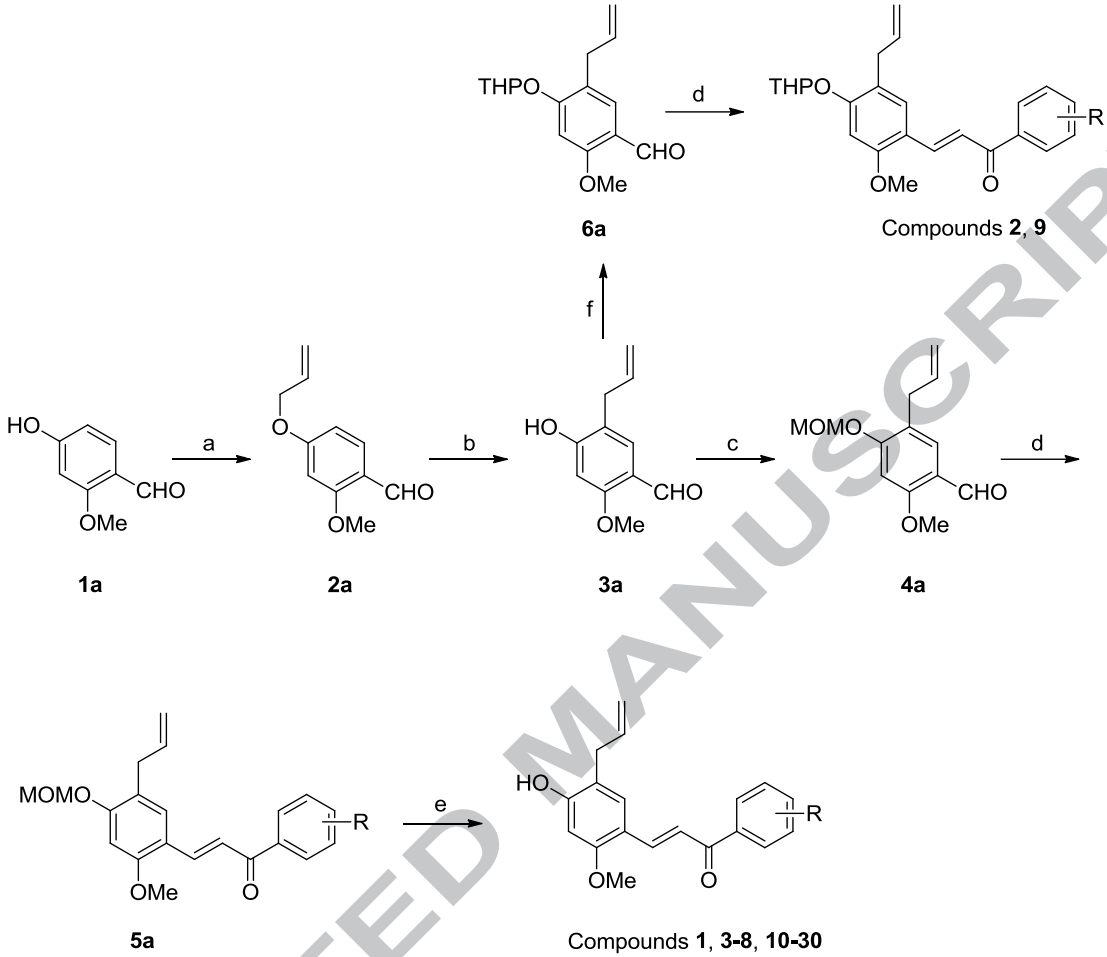

Scheme 1. General synthetic method of the allyl-retrochalcones 1-30. Reagents and conditions: **a)** Allyl bromide, K_2CO_3, acetone, reflux, 6 h; **b)** *N*,*N*-diethylaniline, 200 °C, 10 h; **c)** NaH, MOMCl, THF, 0 °C, 5 h; **d)** Various substituted acetophenones, KOH, EtOH-H_2O (2:1), rt, 4-24 h; **e)** 6N-HCl, MeOH-H2O (2:1), rt, 3-5 h; **f)** 3,4-dihydro-2H-pyran, PPTS, CH_2Cl_2, rt, 4 h.

The syntheses of the allyl-retrochalcones **31-39** are illustrated in Scheme 2. Aldol condensation of **4a** with 1-{4-{[2-(trimethylsilyl)ethoxy]methoxy}phenyl}ethanone in the presence of KOH generated the retrochalcone **7a**, which was subsequently treated with TBAF to give the key intermediate **8a**. Compounds **31-33** were prepared by benzoylation followed by MOM-deprotection. Furthermore, Compound **8a** was alkylated with alkyl bromide in acetone by using K_2CO_3 as a catalyst, and then deprotection of the THP protective groups generated the esters **34**, **36**, and **38**. Finally, they were hydrolyzed with 10% NaOH and 6N-HCl to obtain the carboxylic acids **35**, **37**,

and **39**. All of the new products were isolated by conventional work-up with satisfactory yields. Analytical and spectral data of all synthesized compounds were in full agreement with the proposed structures.

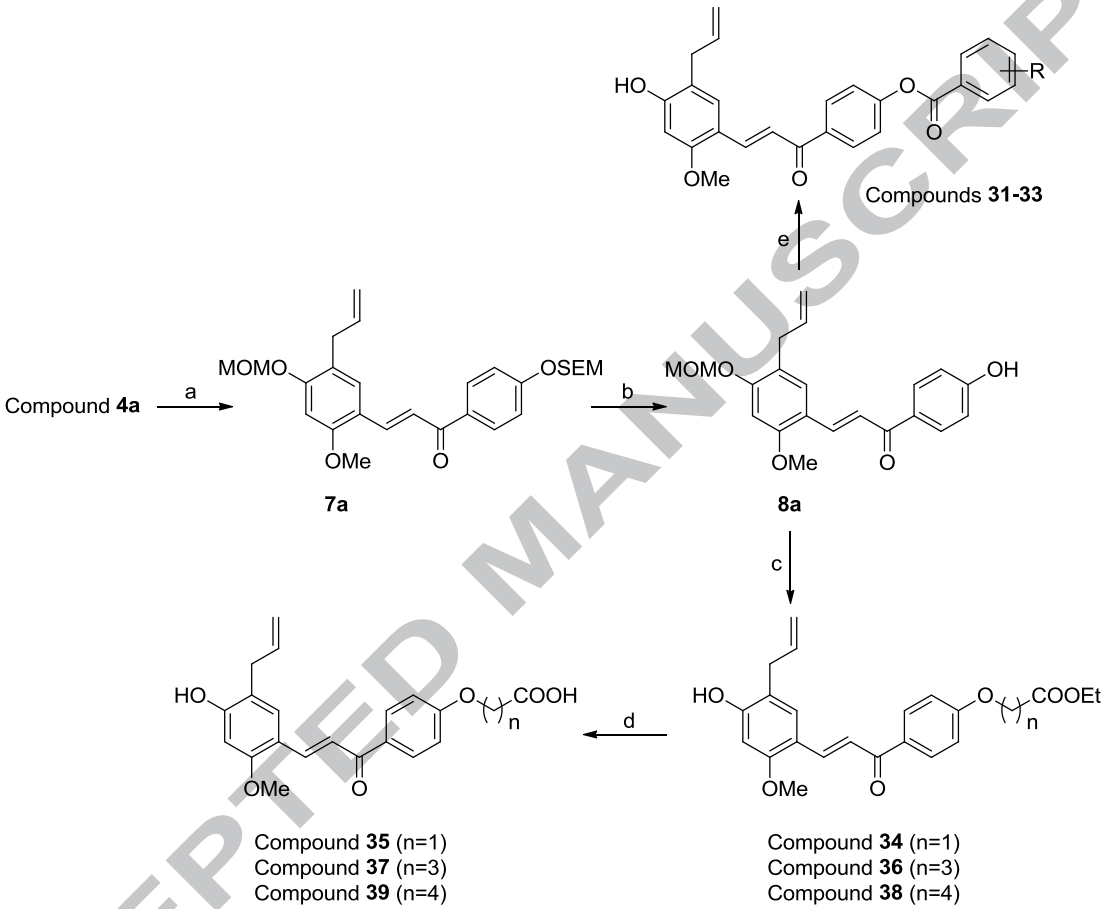

Scheme 2. General synthetic method of the allyl-retrochalcones **31-39**. Reagents and conditions: **a)** 1-{4-{[2-(Trimethylsilyl)ethoxy]methoxy}phenyl}ethanone, KOH, EtOH-H_2O (2:1), rt, overnight; **b)** TBAF, THF, 65 °C, 20 min; **c)** 1) Ethyl 2-bromoacetate, ethyl 4-bromobutanoate, or ethyl 5-bromopentanoate, as well as K_2CO_3 and acetone, 63 °C, 8 h; 2) 6N-HCl, MeOH-H_2O (2:1), rt, 3-5 h. **d)** NaOH (10%), MeOH, rt, 3 h, then 6N-HCl; **e)** 1) Various benzoyl chlorides, Et_3N, THF, rt, 8 h; 2) 6N-HCl, MeOH-H2O (2:1), rt, 3-5 h.

3. Results and discussion

3.1 Inhibitory screening and preliminary structure activity relationship study

The inhibitory activities of the synthesized compounds against PTP1B were assayed using *p*-

nitrophenyl phosphate (*p*NPP) as a substrate, and the results are summarized in Table **1**. Ursolic acid (IC_{50} = 3.1 μM), a known PTP1B inhibitor, was used as a positive control.[18] The all-synthetic compounds, except compounds **4**, **9**, **27**, and **37**, inhibited PTP1B activity in a dose-dependent manner, with IC_{50} values ranging from 0.5 to 24.8 μM. Most of these compounds displayed higher activities than that of licochalcone A. The introduction of an allyl group, instead of a 1,1-dimethylallyl group, at the C-5 position generated Compound **1,** which displayed a two-fold higher inhibitory activity than that of licochalcone A. In contrast, Compound **4**, which bore a *meta*-hydroxyl group on A ring, exhibited no inhibitory effect against PTP1B. Methylation of the obtained Compounds **3** and **5** resulted in higher activities than those of Compounds **1** and **4**, respectively; this observation concurs with our previous results.[16]

Table 1. Inhibitory activities of the synthesized Compounds **1-39** against PTP1B enzyme.

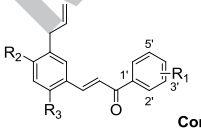

Compounds 1-39

Comp.	R_1	R_2	R_3	PTP1B inhibition[a] IC_{50} (μM)	Comp.	R_1	R_2	R_3	PTP1B inhibition[a] IC_{50} (μM)
1	4'-OH	OMe	OH	12.9 ± 4.7	**22**	4'-$N(Me)_2$	OMe	OH	6.9 ± 0.6
2	4'-OH	OMe	OTHP	9.4 ± 2.5	**23**	3'-$N(Me)_2$	OMe	OH	0.57± 0.2
3	4'-OMe	OMe	OH	7.4 ± 0.9	**24**	2'-$N(Me)_2$	OMe	OH	16.3 ± 3.9
4	3'-OH	OMe	OH	NA	**25**	3'-$N(Me)_2$	OBz	OH	5.0 ± 1.2
5	3'-OMe	OMe	OH	14.6 ± 3.2	**26**	3'-$N(Me)_2$	O-iPr	OH	6.9 ± 1.4
6	2'-OH, 4'-OMe	OMe	OH	24.8 ± 4.3	**27**	3'-$NHSO_2Me$	OMe	OH	NA
7	4'-OEt	OMe	OH	5.3 ± 1.8	**28**	2'-$N(Me)_2$, 4'-OCH_2O-5	OMe	OH	11.8 ± 4.7
8	4'-O-allyl	OMe	OH	5.4 ± 1.2	**29**	3'-$N(allyl)_2$	OMe	OH	4.7 ± 0.1
9	2'-OH, 4'-O-allyl	OMe	OTHP	NA	**30**	4'-$N(allyl)_2$	OMe	OH	5.9 ± 1.6
10	2'-OH, 4'-O-allyl	OMe	OH	6.5 ± 2.4	**31**	4'-(4-*tert*-butyl)benzyloxyl	OMe	OH	5.0 ±1.1
11	4'-O-prenyl	OMe	OH	5.9 ± 0.5	**32**	4'-benzyloxyl	OMe	OH	4.6± 0.6
12	2'-OH, 4'-O-prenyl	OMe	OH	3.0 ± 0.5	**33**	4'-(4-Br)benzyloxyl	OMe	OH	6.6 ± 0.7
13	2'-OMe, 4'-O-prenyl	OMe	OH	3.9 ±1.8	**34**	4'-OCH_2COOEt	OMe	OH	9.4 ± 3.9
14	3'-allyl, 4'-OMe	OMe	OH	10.9 ± 1.4	**35**	4'-OCH_2COOH	OMe	OH	12.6 ± 4.9
15	3'-(2,3-dimethyl)allyl, 4'-OMe	OMe	OH	5.4 ± 0.9	**36**	4'-$O(CH_2)_3COOEt$	OMe	OH	25.6 ± 3.4
16	3'-(3,3-dimethyl)allyl, 4'-OMe	OMe	OH	8.2 ± 3.2	**37**	4'-$O(CH_2)_3COOH$	OMe	OH	32.8 ± 2.9
17	4'-Piperidine	OMe	OH	6.9 ± 1.2	**38**	4'-$O(CH_2)_4COOEt$	OMe	OH	3.9 ± 1.2
18	2'-Piperidine	OMe	OH	9.5 ± 3.4	**39**	4'-$O(CH_2)_4COOH$	OMe	OH	5.8 ± 0.5
19	3'-Piperidine	OMe	OH	7.2 ± 0.5	**40**	Ursolic acid[b]			3.1 ± 1.3
20	4'-Morpholine	OMe	OH	12.3 ± 0.7	**41**	licochalcone A[b]			19.1 ± 0.1
21	4'-pyrazole	OMe	OH	6.3 ± 1.1	**42**	licochalcone E[b]			4.0 ± 0.9

[a] Values are mean of at least n = 3 independent experiments ± SEM.
b Positive control.
NA *means no activity*.

Incorporation of various alkyl groups or allyl groups at the 4-hydroxy position of Compound **5a** yielded compounds with considerably higher activities than that of Compound **1**. For example, the introduction of the ethyl, allyl, and 3,3-dimethylallyl groups at the 4'-hydroxy position of Compound **5a** yielded Compounds **7** (IC_{50} = 5.3 μM), **8** (IC_{50} = 5.4 μM), and **11** (IC_{50} = 5.8 μM), respectively, which showed approximately a two-fold higher inhibitory activity than that of Compound **1** (IC_{50} = 9.4 μM). Insertion of an *ortho* hydroxyl group or methoxy group to the A ring of Compounds **3**, **8**, and **11** generated Compounds **6**, **10**, **12**, and **13**. Interestingly, with an extended substitution at the 4'-hydroxy group, the four retrochalcones, which exhibited a proportionate increase in potency (especially Compound **12** that bore a prenyl group), showed exceptionally good inhibitory activity against PTP1B (IC_{50} = 3.0 μM) compared to that of the positive control, ursolic acid. Consistent with a previous study,[16] protection of Compounds **1** and **10** at the 2'-hydroxy position of their B ring with an THP protective group yielded Compounds **2** and **9**, which showed equivalent or no inhibitory activity against PTP1B. However, by inserting various allyl groups at the C-3' position, Compounds **14**, **15**, and **16** provided similar potency to that of Compound **3** (IC_{50} = 7.4 μM).

Among Compounds **17-19**, which contained piperidine substitution, *meta*- and *para*-substituted derivatives exhibited a more potent PTP1B inhibitory effect than the *ortho*-substituted allyl-retrochalcone **18** (IC_{50} = 9.5 μM). Compound **20** (IC_{50} = 12.3 μM), which had morpholine at its C-4' position, showed a two-fold lower activity than that of Compound **21** (IC_{50} = 6.3 μM), a pyrazole-substituted retrochalcone. In Compounds **22-27**, it was observed that the compounds with *meta*- or *para*-dimethylamino substituents were more potent than those with *ortho*-dimethylamino substituents. More importantly, among these compounds, the *meta*-substituted Compound **23** showed the most significant inhibitory activity against PTP1B, with a low IC_{50} value of 0.57 μM, and exhibited a six-fold higher activity than that of the positive control, ursolic acid.

Incorporation of a benzyl and isopropyl group at the 2'-hydroxy position of A ring generated Compounds 25 (IC_{50} = 5.0 μM) and 26 (IC_{50} = 6.9 μM), but decreased their inhibitory effects. In Compound **27**, incorporation of a methanesulfonamide at its C-3' position resulted in a complete loss of potency. However, Compounds **29** and **30**, which were protected with diallyl groups, showed

strong inhibitory effects similar to that of *p*-allyl in Compound **8** (IC_{50} = 5.4 μM). Compound **1** was benzoylated separately at the 4'-hydroxy group to obtain the retrochalcone derivatives **31-33**, all of which exhibited an approximately two-fold higher activity than the initial Compound **1**. Incorporation of a carboxylic acid residue, as in Compounds **35** and **37**, did not appear to increase the PTP1B inhibition. Compound **39**, however, exhibited moderate potency. Moreover, the other esters (Compounds **34**, **36**, and **38**) displayed varying degrees of PTP1B inhibitory activity. Especially, Compound **38** showed a potent inhibitory effect against PTP1B similar to that of the positive control, ursolic acid. Figure 2 shows the structure-activity relationship of these allyl-retrochalcones.

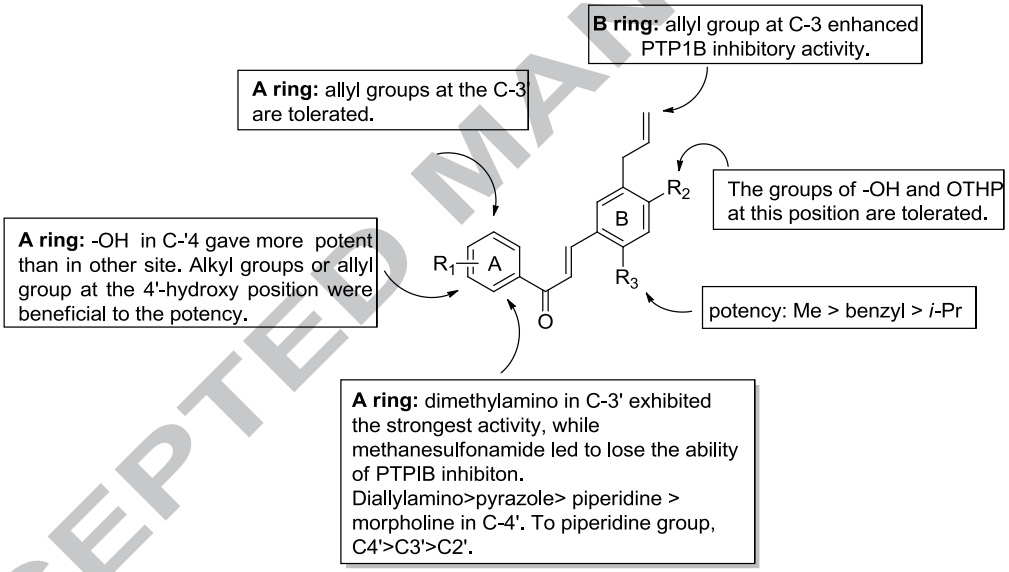

Figure 2. Structure-activity relationships of synthetic allyl-retrochalcones.

3.2 Quantitative evaluation of structure activity relationship (QSAR)

In an attempt to correlate their inhibitory activity against PTP1B with the structure conformation of the synthesized allyl-retrochalcones, a quantitative evaluation of structure activity relationship (QSAR) study was conducted. The materials and methods for this computer-assisted QSAR study are described in our previous publications.[19,20] Our data set consisted of 33 active allyl-retrochalcones, which are shown in Table 1 along with their 50% inhibition concentration (IC_{50}). We used 37 compounds of a total set of 39 synthetic new inhibitors because six allyl-retrochalcones

(Compounds **4**, **6**, **9**, **27**, **36**, and **37**) were excluded due to an inexact IC_{50} concentration, and therefore could not be used in the multiple regression analysis. A statistically significant model of inhibitory activity against PTP1B was obtained with three variables. A scatter plot of predicted values versus experimental values is illustrated in Figure 3.

As shown in Figure 3, an excellent QSAR model was obtained with autocorrelation descriptors (AATS5e, ATSC7c, and ATSC5e), which exhibited a relatively high regression coefficient (R^2_{adj} = 0.74) and was able to describe more than 76% variance in the experimental activity. Autocorrelation descriptor is a molecular descriptor that encodes both the molecular structure and physicochemical properties attributed to atoms as a vector.[21] Autocorrelation of a Topological Structure (ATS) is also known as the Moreau-Broto autocorrelation, and it describes how a property is distributed along a topological structure. AATS5e is the average electronegativity-weighed Moreau-Broto graph spatial autocorrelation coefficient of the fifth lag. ATSC7c is the centered Sanderson charges-weighed Moreau-Broto graph spatial autocorrelation coefficient of the seventh lag, ATSC5e represents the centered Sanderson electronegativity-weighed Moreau-Broto graph spatial autocorrelation coefficient of the fifth lag.[22,23] The QSAR results indicated that electronegativity and molecular charges might play an important role in the inhibitory activities of the synthesized allyl-retrochalcones against PTP1B.

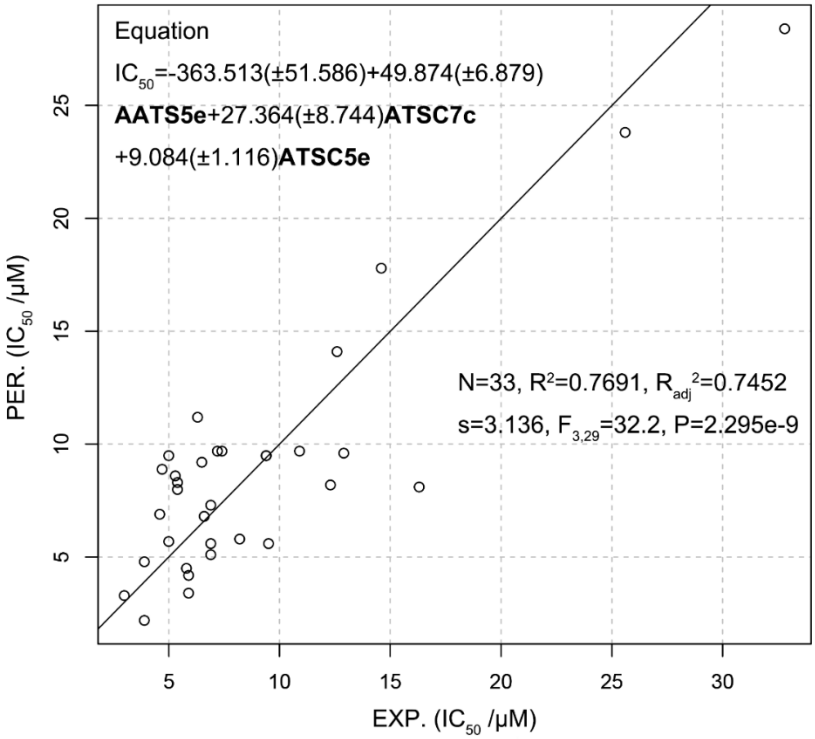

Figure 3. Scatter plot of predicted activity against the corresponding experimental activity. N is the number of compounds considered in the regression, R^2 is the multiple correlation coefficient, R^2_{adj} is the adjusted multiple correlation coefficient, s is residual standard error, and the F value is related to the F-statistical analysis (Fischer test). Numbers in parentheses indicate the standard deviation of the coefficients. p refers to the significance of the variables in the model.

On the basis of the SAR and QSAR results, we concluded that the inhibitory activities of the allyl-retrochalcones against PTP1B may reveal valuable information regarding compound structure-activity relationship for the development of novel PTP1B inhibitors.

3.3 Cellular screening of active Compound 23

Glucose influx into cells is regulated by the insulin receptor (IR) transduction pathway. Dysregulation of its downstream molecules (e.g. insulin receptor substrate 1 and Akt) contribute to insulin resistance in the liver.[24,25] Considering that PTP1B is a negative regulator of the insulin signaling pathway, active Compound **23** would activate insulin receptor substrate-1 (IRS-1) and protein kinase B (Akt) to revert insulin resistance. Therefore, we assessed the effect of **23** in

palmitate acid (PA)-induced insulin resistant HepG2 cells. As shown in Figure 4A, incubation with PA significantly downregulated phospho-IRS-1 (P-IRS-1) and phospho-Akt (P-Akt) in HepG2 cells, compared with single insulin stimulation. However, treatment with Compound **23** at concentrations of 5 and 10 μM markedly enhanced P-IRS1 and P-Akt, respectively. The results indicated that Compound **23** can alleviate PA-induced insulin resistance in the liver.

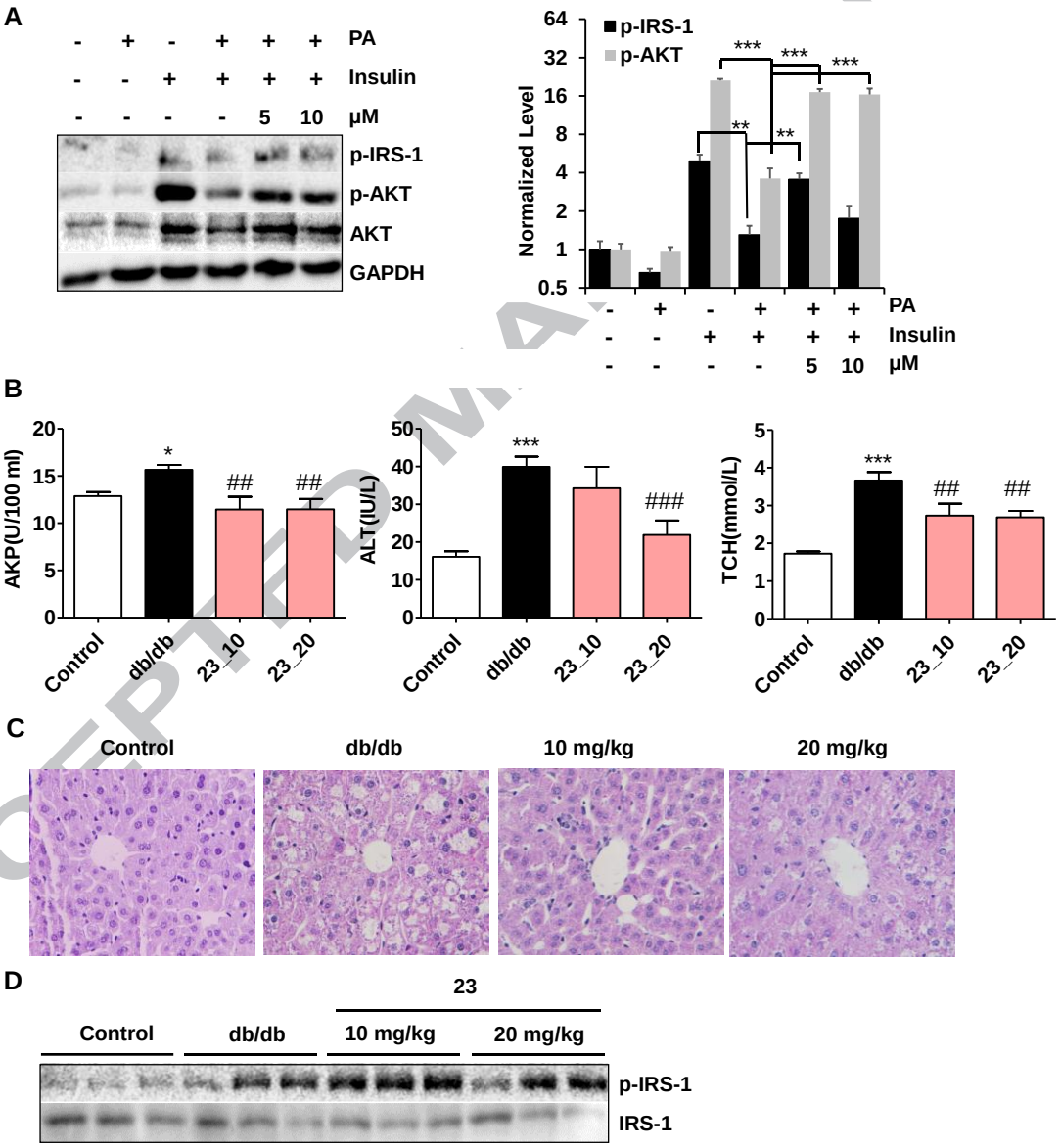

Figure 4. Compound **23** alleviated palmitate acid (PA)-induced insulin resistance *in vitro*, and relieved liver injury *in vivo*. (**A**) HepG2 cells were pretreated with or without **23** at the indicated concentrations for 1 h, and then incubated with or without 0.15 mM PA for another 24 h. Finally, the

cells were stimulated with or without 100 nM insulin for 5 min before being harvested. The lysates were subjected to an immunoblotting assay, as described in the Methods section. The blots were quantified and plotted. **, P < 0.01; ***, P< 0.001. (**B**) Eight-week-old db/db mice were orally administered 10 or 20 mg/kg of **23** or vehicle every other-day for 10 weeks. The mice were sacrificed, and their serum and liver samples were collected. AKP, ALT, and TCH levels were measured using standard assay kits, as mentioned in the Method section. **(C)** Liver samples were subjected to an H&E staining assay. (**D**) Liver lysates were immunoblotted for p-IRS1. db/db vs. Control. *, P < 0.05; ***, P < 0.001; 23 vs. db/db, ##, P < 0.01; ###, P < 0.001.

3.4 *In vivo* evaluation of Compound 23

Next, because insulin resistance and liver injury are closely associated, we investigated the potential protective effect of Compound **23** against hyperglycemia-induced liver injury in type 2 diabetic db/db mice. As shown in Figure 4B, the levels of alkaline phosphatase (AKP) and alanine aminotransferase (ALT), classical markers for liver function and integrity, respectively, were remarkably increased in db/db mice. After treatment with Compound **23** at 10 and 20 mg/kg, AKP and ALT contents markedly decreased. In addition, the administration of Compound **23** effectively and significantly downregulated the level of total cholesterol (TCH) in the serum.

Histological examination results showed diffuse lipid accumulation and sporadic large lipid droplets in the liver tissues of db/db mice. However, Compound **23** (10 and 20 mg/kg) treatment significantly attenuated the extent of steatosis, as shown in Figure 4C. The size and number of these lipid droplets in the liver were also notably reduced, suggesting that Compound **23** effectively inhibited lipid accumulation in the liver and exerted a significant hepatoprotective effect. Meanwhile, the levels of phosphorylated IRS-1 in liver extracts were closely related to the activation of IR signaling observed in the livers, in spite of individual differences were observed (Figure 4D). These data indicated that the activation of IR signaling pathway by Compound **23** protected mice from liver injury.

3.5 Pharmacokinetic study for Compound 23

With these encouraging *in vitro* and *in vivo* results, Compound **23** was further subjected to preliminary pharmacokinetic profiling in Sprague-Dawley (SD) rats. Compound **23** was administered at 2 mg/kg intravenously or at 20 mg/kg orally to male SD rats. The pharmacokinetic parameters are summarized in Figure 5A. Rats intravenously administered **23** exhibited prolonged half-life (21.12 h) and low clearance rate (1.41 mL/min/kg). In contrast, rats orally administered **23** at 20 mg/kg showed moderate oral exposure ($AUC_{0-\infty}$= 1620.78 h.ng/mL), half-life (8.85 h), and high C_{max} (2148.83 ng/mL). Interestingly, there was a second peak at 4 h after intragastric administration (Figure 5B-5C), probably because hepatoenteric circulation caused part of the drug to be absorbed once again in the intestine.

A

	Dose (mg/kg)	AUC (0-t)	AUC (0-∞)	t1/2z (h)	T_{max} (h)	Vz/F	CLz/F	C_{max} (ng/ml)
i.v.	2	1434.56	1620.78	21.12	0.08	31.97	1.41	2148.83
p.o.	20	583.70	605.52	8.85	14.00	482.41	36.12	46.19

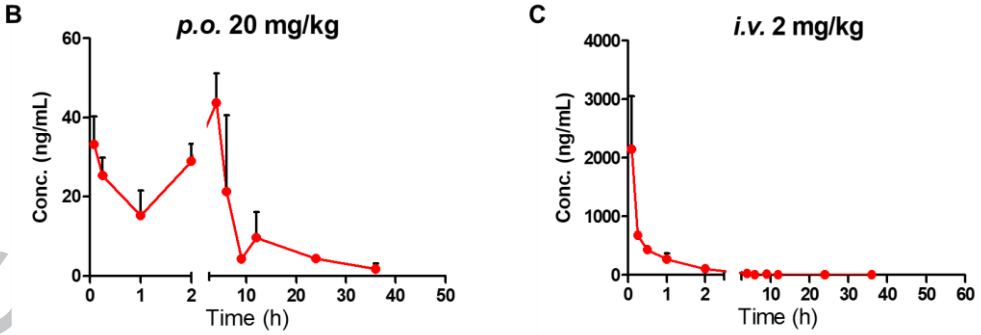

Figure 5. (A) Pharmacokinetic parameters of Compound **23** in rats. **(B)** Mean plasma concentration-time profile of Compound **23** at a single oral dose of 20 mg/kg. **(C)** Mean plasma concentration-time profile of Compound **23** at a single intravenous dose of 2 mg/kg. Plots are mean ± SD (n = 3 in each group).

3.6 Molecular docking and molecular dynamics simulation

Because it is not known whether Compound **23** specifically targets the catalytic site or a second phosphor-tyrosine-binding pocket near the catalytic site (which has been proposed to be a considerable binding site to promote selectivity and affinity[26]), we adopted a complex of PTP1B and a selective inhibitor as a reference structure to cross the two binding pockets (PDB ID 1Q1M). The results of the docking study clearly showed that the active Compound **23** was a catalytic site-specific inhibitor because the top 20 positions were all enriched in this pocket and in nearby areas.

For further insight into the intermolecular binding mode, we performed a 50-ns molecular dynamics simulation. As shown in Figure 6A, the receptor and ligand converged after 20 ns and the root mean square deviation of the backbone atoms was about 1.6 Å and 2.0 Å, respectively. Unexpectedly, the ligand showed a sudden conformational transition from 10 to 13 ns, indicating that the docking result was not the authentic final conformation because the flexibility of the protein receptor is not considered in the half-rigid docking. By analyzing the trajectory, we found that during the conformational transition of the ligand, the configuration of the catalytic pocket also started to reform. Figures 6A and 6B clearly show that a conserved protein loop (the WPD-loop) transformed from a closed (hydrolysis competent) to an open (hydrolysis incompetent) position, whereas the protein tyrosine phosphatase (PTP) loop, which contains the catalytic cysteine CYS215, showed no significant change. Previous research has shown that the WPD loop plays a central role in the mechanism of PTP1B catalysis. In the apo form, WPD loop is usually in an “open” conformation, whereas it closes over the active site upon ligand binding, and its motion is the rate-limiting step for hydrolysis.[27] The result of this simulation is closely consistent with the results that indicated that our compound has favorable affinity to and reasonable binding mode targeting at the catalytic site of PTP1B.

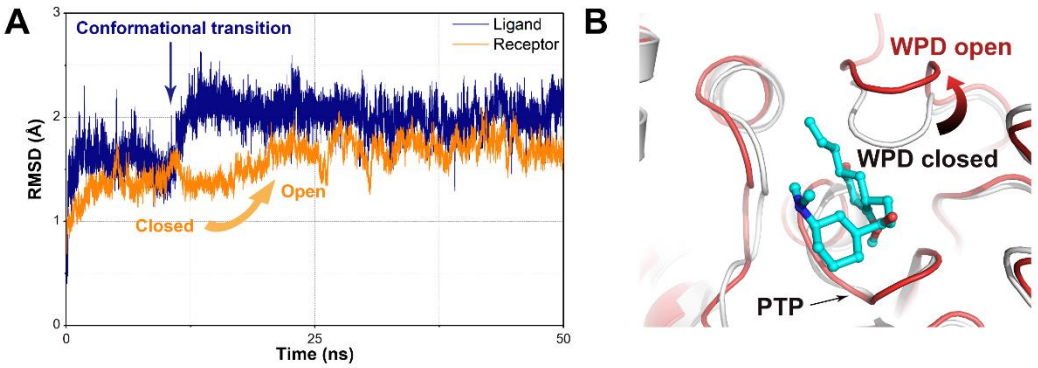

Figure 6. Conformational transition during simulation. **(A)** Backbone root mean square deviations are shown as a function of time for ligand (blue) and receptor (yellow). **(B)** WPD loop transformed from a closed (grey) to an open (red) position.

Although conformational changes that occur upon substrate binding have been well characterized,[28] the mechanisms of small-molecular inhibition are still ambiguous. Hence, we performed molecular mechanics/generalized born surface area (MM/GBSA) and calculation of binding free energy to determine the inherent driving force of conformational transition. Trajectories of 2-10 and 40-50 ns were chosen as representatives to calculate energy before and after transition, respectively. Total binding energies (which were -54.6740 ± 4.2343 kcal/mol before and -53.6279 ± 5.4268 kcal/mol after) did not change significantly, but conformation and per-residue energy contribution exhibited considerable differences. Figures 7A-7B show the top 10 contributing residues, whereas Figures 7C-7D show the corresponding values. The ligand obtained a further step insert in the catalytic pocket, and the energy contributions of ARG221 and SER216 slightly decreased. By examining energy components, we found that electrostatic contribution was the dominant term, consistent with the formation of hydrogen bonds. Consequently, although docking task can indicate binding site and provide binding structure, its inherent limitation is that it cannot reveal the in-depth mechanism. During the molecular simulation, the electrostatic contribution of ARG221 and SER216 was the driving force that facilitated the conformational transition of the ligand, as well as the motion of the WPD loop. Thereafter, the hydrolysis ability of PTP1B in a complex with Compound **23** to prevent the development of some diseases was no longer available.

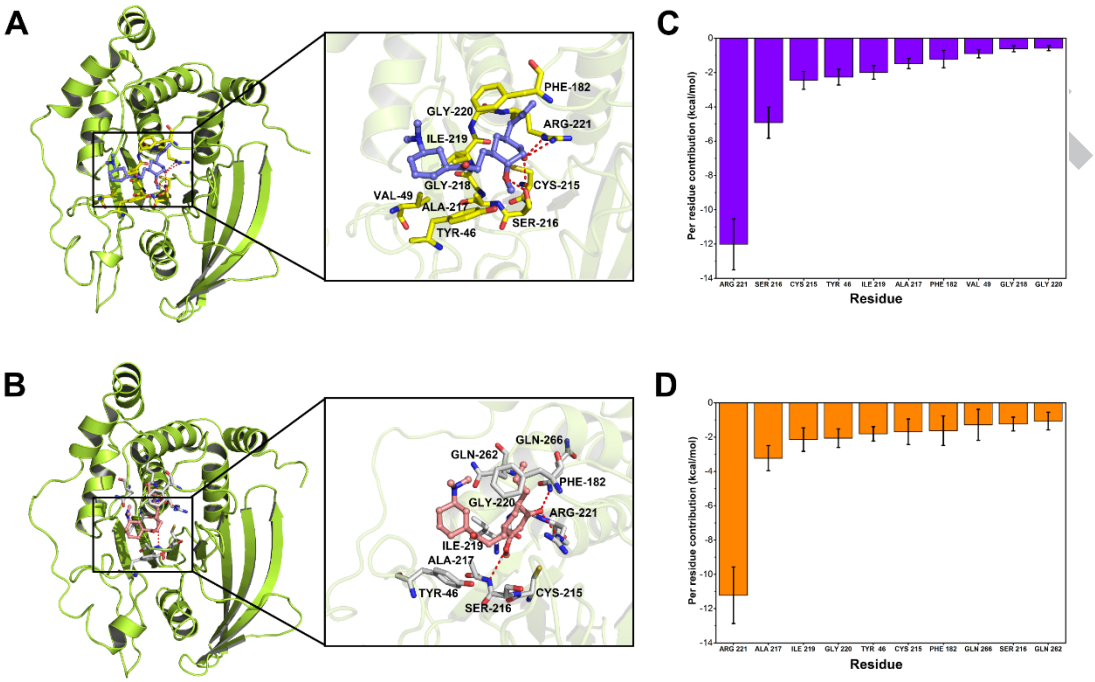

Figure 7. Dynamic and energy changes before and after conformational transition. **(A, C)** Mapping of the energetically important residues (yellow) before transition and the corresponding values. **(B, D)** Mapping of the energetically important residues (grey) after transition and the corresponding values.

4. Conclusion

In conclusion, in the present study, we synthesized and investigated the inhibitory activity of new allyl-retrochalcones against PTP1B. Among the allyl-retrochalcone derivatives, compounds **7**, **8**, **11**, **15**, **25**, **29**, **30**, **31**, **32**, and **39** exhibited moderate inhibitory effects, with IC_{50} values ranging from 4.6 to 5.9 µM. The other four compounds, **12**, **13**, **23**, and **38**, showed potent inhibition against PTP1B compared with the positive control, ursolic acid (IC_{50} = 3.1 µM). Among all the synthesized compounds, **23** was the most active PTP1B inhibitor, with an IC_{50} value of 0.57 µM, nearly six-fold higher than that of the positive control. Additionally, the allyl-retrochalcones with benzoylation at the 4-hydroxy group position showed promising inhibitory properties against PTP1B. The above results suggested a starting point for further optimization of retrochalcones having an allyl group substitution at position C-5 as PTP1B inhibitors. The results of quantitative SAR analyses suggested

that the electronegativity and molecular charges of the compounds were closely correlated with their PTP1B inhibition.

Further studies on cellular activities revealed that Compound **23** could activate IRS-1 and Akt to revert PA-stimulated insulin resistance in HepG2 cells. The results of our *in vivo* examination in db/db mice identified Compound **23,** the most potent compound, as a new active inhibitor with an ability to prevent hyperglycemia-induced liver injury and insulin sensitization. The results of docking analysis and molecular dynamics simulation indicated that Compound **23** had favorable affinity to and reasonable binding mode targeting at the catalytic site of PTP1B. The novel compounds reported in this study will provide new insights to the design and development of new low-molecular-weight PTP1B inhibitors.

5. Experimental section

5.1 Chemistry

5.1.1 General

Solvents were distilled under positive pressure of dry argon before use and dried using standard methods. Unless otherwise noted, chemicals were obtained from local suppliers and were used without further purification. All reactions were monitored by thin-layer chromatography (250 μ silica gel 60 F_{254} glass plates). Column chromatography was conducted using a Merck silica gel 60 column (230-400 mesh ASTM; Merck KGaA, Darmstadt, Germany). Melting points were determined using a Fisher-Johns melting apparatus and uncorrected. Proton nuclear magnetic resonance (^{1}H NMR and ^{13}C NMR) spectra were recorded on a Bruker 500 MHz spectrometer. Chemical shifts were presented as parts per million with tetramethylsilane (TMS) as an internal reference. Electron-spray ionization mass spectra in positive mode (ESI-MS) data were recorded on a Bruker Esquire 3000t spectrometer.

5.1.2 4-(Allyloxy)-2-methoxybenzaldehyde (2a). Potassium carbonate (68.1 g, 0.48 mol) was

added slowly to a solution of 4-hydroxy-2-methoxybenzaldehyde (**1a**; 25.0 g, 0.16 mol) and 3-bromoprop-1-ene (38.1 g, 0.32 mol) in acetone (150 mL). The reaction mixture was refluxed for 6 h. The resulting mixture was filtered and the filtrate was concentrated under reduced pressure. The residue was then dissolved in EtOAc (50 mL) and washed with water (50 mL) and brine (50 mL). The organic layer was dried over $MgSO_4$, filtered, and concentrated under reduced pressure. The residue was purified by chromatography on silica gel to obtain Compound **2a** (27.95 g, 91%) as a light yellow liquid. ^{1}H-NMR (400 MHz, acetone--d_6) δ (ppm): 10.26 (s, 1H), 7.73 (s, *J* = 1.5 Hz, 1H), 6.74 (s, 1H), 6.72 (d, *J* = 1.5 Hz, 1H), 6.13-6.03 (m, 1H), 5.48 (dq, *J* = 17.3, 1.7 Hz, 1H), 5.33 (dq, *J* = 10.6, 1.4 Hz, 1H), 4.74 (d, *J* = 5.3 Hz, 2H), 3.98 (s, 3H).

5.1.3 5-Allyl-4-hydroxy-2-methoxybenzaldehyde (3a). A solution of **2a** (25.0 g, 0.13 mol) in *N,N*-diethylaniline (50 mL) was heated at 200 °C under nitrogen atmosphere for 10 h. The resulting mixture was purified by chromatography on silica gel to obtain the desired compound, **3a** (5.24 g, 21%), as brownish red solid. m.p: 99.6-101.3 °C. ^{1}H-NMR (400 MHz, acetone--d_6) δ (ppm): 10.26 (s, 1H), 7.57 (s, 1H), 6.65 (s, 1H), 6.20-5.79 (m, 1H), 5.11 (dd, *J* = 17.1, 2.0 Hz, 1H), 5.07-5.02 (m, 1H), 3.91 (s, 3H), 3.37 (d, *J* = 6.6 Hz, 2H).

5.1.4 5-Allyl-2-methoxy-4-(methoxymethoxy)benzaldehyde (4a). A solution of 60% sodium hydride (2.2 g, 0.056 mol) in dry THF (100 mL) was added portionwise to a solution of **3a** (5.24 g, 0.028 mol) in THF (10 mL), followed by chloromethyl methyl ether (4.3 mL, 0.056 mol) in an ice-bath. After 5 h, the resulting mixture was quenched with saturated ammonium chloride solution and extracted with EtOAc (3 × 100 mL). The combined organic layers were washed with water (150 mL), dried over $MgSO_4$, and concentrated under reduced pressure. The residue was further purified by chromatography on silica gel to obtain the desired 5-allyl-2-methoxy-4-

(methoxymethoxy)benzaldehyde (**4a,** 5.24 g, 80%) as a yellow solid. m.p: 85.3-87.9 °C. ^{1}H-NMR (400 MHz, acetone--d_6) δ (ppm): 10.15 (s, 1H), 7.40 (s, 1H), 6.76 (s, 1H), 6.01-5.63 (m, 1H), 5.24 (d, *J* = 19.0 Hz, 2H), 4.93 (dd, *J* = 17.1, 1.5 Hz, 1H), 4.89 (d, *J* = 10.5 Hz, 1H), 3.81 (s, 3H), 3.35 (s, 3H), 3.21 (d, *J* = 6.6 Hz, 2H).

5.1.5 (*E*)-3-[5-Allyl-2-methoxy-4-(methoxymethoxy)phenyl]-1-phenylprop-2-en-1-one (5a). KOH solution (44.0 mg, 0.8 mmol) in H_2O (1 mL) was added dropwise to a stirred solution of **4a** (0.1 g, 0.42 mmol) in EtOH and H_2O (9 mL, v/v 2:1) at room temperature. The reaction mixture was stirred at room temperature for 4-24 h. The resulting mixture was diluted with H_2O (15 mL) and extracted with EtOAc (3× 20 mL). The combined organic layers were washed with brine (15 mL) and dried over anhydrous $MgSO_4$, filtered, and concentrated under reduced pressure. The residue was further purified by chromatography on silica gel to obtain the desired Compound **5a** with a yield of 35-89%.

5.1.6 General preparation procedure of the compounds 1, 3-8 and 10-30.

Ten drops of 6*N*-HCl was added to several solutions of **5a** (0.1 mmol) in MeOH and H_2O (10 mL, v/v 2:1). The reaction mixture was stirred at room temperature for 3-5 h, quenched with saturated aqueous NH_4Cl solution (10 mL) and extracted with EtOAc (3 × 10 mL). The combined organic layers were washed with water (20 mL) and brine (20 mL), dried over $MgSO_4$, filtered, and concentrated under reduced pressure. The residue was purified by chromatography on silica gel to obtain the target compounds below.

5.1.6.1 (*E*)-3-(5-Allyl-4-hydroxy-2-methoxyphenyl)-1-(4-hydroxyphenyl)prop-2-en-1-one (1). Yellow solid, 42.64% yield, m.p: 101.1-102.4 °C. ^{1}H-NMR (500 MHz, acetone--d_6) δ (ppm): 8.98 (s,

1H), 8.73 (s, 1H), 7.92 (d, *J* = 15.7 Hz, 1H), 7.88 (d, *J* = 8.6 Hz, 2H), 7.55 (d, *J* = 15.6 Hz, 1H), 7.47 (s, 1H), 6.82 (d, *J* = 8.5 Hz, 2H), 6.47 (s, 1H), 5.90 (dd, *J* = 16.7, 10.1 Hz, 1H), 4.93 (dd, *J* = 17.1, 1.7 Hz, 1H,- -), 4.87 (d, *J* = 8.9 Hz, 1H), 3.74 (s, 3H, -OCH_3), 3.22 (d, *J* = 6.5 Hz, 2H). ^{13}C-NMR (125 MHz, acetone-d_6) δ (ppm): 188.4, 162.4, 159.9, 159.4, 139.4, 138.1, 131.9, 131.6 ×2, 131.4, 120.2, 119.6, 116.7, 116.1 ×2, 115.4, 99.9, 56.0, 34.2. ESI-MS *m/z*: 311.18 $(M+H)^+$, calcd for $C_{19}H_{18}O_4$: 310.12.

5.1.6.2 (*E*)-3-(5-Allyl-4-hydroxy-2-methoxyphenyl)-1-(4-methoxyphenyl)prop-2-en-1-one (3). Yellow solid, 49.5% yield, m.p: 123.2-125.1 °C. ^{1}H-NMR (500 MHz, acetone-d_6) δ (ppm): 8.79 (s, 1H), 7.96 (s, 1H), 7.93 (d, *J* = 5.6 Hz, 1H), 7.91 (s, 1H), 7.57 (d, *J* = 15.6 Hz), 7.49 (s, 1H), 6.91 (d, *J* = 8.8 Hz, 2H), 6.47 (s, 1H), 5.90 (dd, *J* = 16.7, 1.7 Hz, 1H), 4.93 (dd, *J* = 17.1, 1.7 Hz), 4.87 (d, *J* = 8.9 Hz, 1H), 3.76 (s, 3H), 3.74 (s, 3H), 3.22 (d, *J* = 6.5 Hz, 2H). ^{13}C-NMR (125 MHz, acetone-d_6) δ (ppm): 188.5, 164.1, 159.9, 159.5, 139.6, 138.1, 132.7, 131.4, 131.3 ×2, 120.2, 119.5, 115.6, 115.4, 114.6 ×2, 99.9, 56.1, 55.8, 34.2. ESI-MS *m/z*: 325.14 $(M+H)^+$, calcd for $C_{20}H_{20}O_4$: 324.14.

5.1.6.3 (*E*)-3-(5-Allyl-4-hydroxy-2-methoxyphenyl)-1-(3-hydroxyphenyl)prop-2-en-1-one (4). Yellow solid, 47.98% yield, m.p: 105.5-107.3 °C. ^{1}H-NMR (500 MHz, acetone-d_6) δ (ppm): 8.73 (s, 2H), 7.93 (d, *J* = 15.6 Hz, 1H), 7.51 (s, 1H), 7.48 (d, *J* = 2.3 Hz, 1H), 7.42 (d, *J* = 7.6 Hz, 1H), 7.38 (s, 1H), 7.23 (d, *J* = 7.9 Hz, 1H), 6.95 (d, *J* = 8.0 Hz, 1H), 6.49 (s, 1H), 5.90 (dd, *J* = 16.7, 6.5 Hz, 1H), 4.93 (dd, *J* = 17.1, 1.7 Hz, 1H), 4.87 (d, *J* = 8.9 Hz, 1H), 3.74 (s, 3H), 3.22 (d, *J* = 6.5 Hz, 2H). ^{13}C-NMR (125 MHz, acetone-d_6) δ (ppm): 190.0, 160.0, 159.7, 158.6, 141.4, 140.3, 138.0, 131.5, 130.4, 120.4, 120.2, 119.6, 116.3, 115.5, 115.4, 99.9, 66.0, 56.0, 34.1. ESI-MS *m/z*: 311.24 $(M+H)^+$, calcd for $C_{19}H_{18}O_4$: 310.12.

5.1.6.4 (*E*)-3-(5-Allyl-4-hydroxy-2-methoxyphenyl)-1-(3-methoxyphenyl)prop-2-en-1-one (5). Yellow solid, 45.8% yield. m.p: 139.0-141.5 °C. ^{1}H NMR (500 MHz, acetone-d_6) δ (ppm): 8.91 (s, 1H), 7.93 (d, *J* = 15.6 Hz, 1H), 7.57 (d, *J* = 1.8 Hz, 1H), 7.51 (d, *J* = 2.1 Hz, 1H), 7.50 (s, 1H), 7.43 (d, *J* = 1.6 Hz, 1H), 7.31 (t, *J* = 7.9 Hz, 1H), 7.04 (dd, *J* = 8.2, 2.1 Hz, 1H), 6.48 (s, 1H), 5.90 (dd, *J* = 16.7, 6.5 Hz, 1H), 4.93 (dd, *J* = 17.1, 1.7 Hz, 1H), 4.87 (d, *J* = 8.9 Hz, 1H), 3.74 (s, 6H), 3.22 (d, *J* = 6.5 Hz, 2H). ^{13}C-NMR (125 MHz, acetone-d_6) δ (ppm): 190.0, 160.9, 160.4, 159.8, 141.2, 140.5, 138.0, 131.5, 130.4, 121.4, 120.2, 119.5, 119.1, 116.3, 115.4, 113.8, 99.8, 56.0, 55.7, 34.1. ESI-MS *m/z*: 325.32 $(M+H)^+$, calcd for $C_{20}H_{20}O_4$: 324.14.

5.1.6.5 (*E*)-3-(5-Allyl-4-hydroxy-2-methoxyphenyl)-1-(2-hydroxy-4-methoxyphenyl)prop-2-en-1-one (6). Yellow solid, 42.7% yield, m.p: 134.4-136.3 °C. ^{1}H-NMR (500 MHz, acetone-d_6) δ (ppm): 8.83 (s, 1H), 8.31 (s, 1H), 7.93 (d, *J* = 15.6 Hz, 1H), 7.59 (d, *J* = 1.8 Hz), 7.57 (d, *J* = 1.8 Hz, 1H), 7.52 (d, *J* = 1.6 Hz, 1H), 7.48 (s, 1H), 6.81 (d, *J* = 8.2 Hz, 1H), 6.48 (s, 1H), 5.90 (dd, *J* = 16.7, 6.5 Hz, 1H), 4.93 (dd, *J* = 17.1, 1.7 Hz, 1H), 4.87 (d, *J* = 8.9 Hz, 1H), 3.80 (s, 3H), 3.74 (s, 3H), 3.22 (d, *J* = 6.5 Hz, 2H. ^{13}C-NMR (125 MHz, acetone-d_6) δ (ppm): 186.9, 158.4, 158.0, 150.5, 147.1, 138.9, 136.7, 130.7, 129.9, 122.5, 118.7, 118.0, 115.2, 113.9, 113.9, 110.6, 99.4, 54.9, 54.6, 32.7. ESI-MS *m/z*: 341.07 $(M+H)^+$, calcd for $C_{20}H_{20}O_5$: 340.13.

5.1.6.6 (*E*)-3-(5-Allyl-4-hydroxy-2-methoxyphenyl)-1-(4-ethoxyphenyl)prop-2-en-1-one (7). Yellow solid, 49.5% yield, m.p: 131.3-132.8 °C. ^{1}H-NMR (500 MHz, acetone--d_6) δ (ppm): 8.87 (s, 1H), 7.95 (s, 1H), 7.93 (d, *J* = 15.6 Hz, 1H), 7.57 (d, *J* = 15.6 Hz, 1H), 7.53 (d, *J* = 8.4 Hz, 1H), 7.49 (s, 1H), 6.89 (d, *J* = 8.7 Hz, 2H), 6.47 (s, 1H), 5.90 (dd, *J* = 16.7, 6.5 Hz, 1H), 4.93 (dd, *J* = 17.1, 1.7 Hz, 1H), 4.87 (d, *J* = 8.9 Hz, 1H), 4.01 (dd, *J* = 13.9, 6.9 Hz, 2H), 3.76 (s, 3H), 3.22 (d, *J* = 6.5 Hz, 2H), 1.26 (t, *J* = 6.9 Hz, 3H). ^{13}C-NMR (125 MHz, acetone-d_6) δ (ppm): 188.5, 163.4, 159.8, 159.5,

139.5, 138.1, 132.5, 131.4, 131.3, 120.1, 119.4, 116.5, 115.3, 115.0 ×2, 99.8, 64.4, 56.0, 34.1, 14.9. ESI-MS *m/z*: 339.23 $(M+H)^+$, calcd for$C_{21}H_{22}O_4$: 338.15.

5.1.6.7 (*E*)-3-(5-Allyl-4-hydroxy-2-methoxyphenyl)-1-[4-(allyloxy)phenyl]prop-2-en-1-one (8). Yellow solid, 56.87% yield, m.p: 103.4-105.2 °C. ^{1}H NMR (500 MHz, acetone-d_6) δ (ppm): 8.85 (s, 1H), 7.94 (dd, *J* = 11.3, 2.6 Hz, 3H), 7.56 (d, *J* = 15.6 Hz, 1H), 7.48 (s, 1H), 6.92 (d, *J* = 8.2 Hz, 2H), 6.47 (s, 1H), 6.00-5.83 (m, 2H), 5.30 (d, *J* = 17.3 Hz, 1H), 5.14 (d, *J* = 10.4 Hz, 1H), 4.93 (dd, *J* = 17.1, 1.7 Hz, 1H), 4.87 (d, *J* = 8.9 Hz, 1H), 4.53 (d, *J* = 4.4 Hz, 2H), 3.74 (s, 3H), 3.22 (d, *J* = 6.5 Hz, 2H). ^{13}C-NMR (125 MHz, acetone-d_6) δ (ppm): 188.5, 163.0, 159.5, 139.7, 138.0, 134.2, 133.7, 131.9, 131.4, 131.3, 129.6, 120.2, 119.4, 117.8, 116.6, 115.5, 115.3, 99.9, 69.3, 66.9, 56.06, 34.1. ESI-MS *m/z*: 351.22 $(M+H)^+$, calcd for $C_{22}H_{22}O_4$ 350.15.

5.1.6.8 (*E*)-3-(5-Allyl-4-hydroxy-2-methoxyphenyl)-1-[4-(allyloxy)-2-hydroxyphenyl]prop-2-en-1-one (10). Yellow solid, 47.98% yield, m.p: 129.1-132.2 °C. ^{1}H-NMR (500 MHz, acetone-d_6) δ (ppm): 8.07 (d, *J* = 15.6 Hz, 1H), 7.93 (d, *J* = 9.4 Hz, 1H), 7.65 (dd, *J* = 9.7, 5.8 Hz, 1H), 7.53 (s, 1H, Ar-H), 6.50 (s, 1H), 6.43 (d, *J* = 15.6 Hz, 1H), 6.33 (s, 1H), 6.01-5.80 (m, 2H), 5.30 (d, *J* = 17.2 Hz, 1H), 5.15 (d, *J* = 9.1 Hz, 1H), 4.93 (dd, *J* = 17.1, 1.7 Hz, 1H), 4.87 (d, *J* = 8.9 Hz, 1H), 4.53 (d, *J* = 4.4 Hz, 2H), 3.74 (s, 3H), 3.22 (d, *J* = 6.5 Hz, 2H), ^{13}C-NMR (125 MHz, acetone-d_6) δ (ppm): 193.3, 187.4, 160.6, 160.1, 140.8, 138.0, 134.9, 132.9, 132.5, 131.9, 120.3, 118.0, 117.7, 116.2, 115.4, 109.3, 102.5, 99.7, 99.3, 69.6, 56.1, 34.1. ESI-MS *m/z*: 367.23 $(M+H)^+$, calcd for $C_{22}H_{22}O_5$: 366.15.

5.1.6.9 (*E*)-3-(5-Allyl-4-hydroxy-2-methoxyphenyl)-1-{4-[(3-methylbut-2-en-1-yl)oxy]phenyl}prop-2-en-1-one. Yellow solid, 45.2% yield, m.p: 108.2-111.1 °C. ^{1}H NMR (500 MHz, acetone-d_6) δ (ppm): 8.92 (s, 1H), 8.00 (d, *J* = 8.5 Hz, 1H), 7.98-7.95 (m, 2H), 7.94 (s, 1H),

7.63-7.58 (m, 1H), 7.51 (d, *J* = 4.9 Hz, 3H), 7.25 (d, *J* = 8.5 Hz, 2H), 6.44 (s, 1H), 5.90 (dd, *J* = 16.7 Hz, 6.5 Hz, 1H), 4.93 (dd, *J* = 17.1, 1.7 Hz), 4.87 (d, *J* = 8.9 Hz, 1H), 3.73 (s, 3H), 3.22 (d, *J* = 5.8 Hz, 2H), 1.80 (s, 3H, -CH_3), 1.68 (s, 3H, -CH_3). ^{13}C-NMR (125 MHz, acetone-d_6) δ (ppm): 188.8, 165.2, 160.1, 159.7, 158.4, 155.3, 140.4, 137.9, 131.8, 131.6, 130.4, 130.1, 129.6, 127.5, 122.94, 119.6, 119.3, 116.2, 115.4, 99.8, 56.0, 41.5 ×2, 34.1. ESI-MS *m/z*: 379.55 $(M+H)^+$, calcd for $C_{24}H_{26}O_4$: 378.18.

5.1.6.10 (*E*)-3-(5-Allyl-4-hydroxy-2-methoxyphenyl)-1-{2-methoxy-4-[(3-methylbut-2-en-1-yl)oxy]phenyl}prop-2-en-1-one (12). Yellow solid, 47.4% yield, m.p: 116.3-118.2 °C. ^{1}H-NMR (500 MHz, acetone-d_6) δ (ppm): 8.75 (s, 1H), 8.41 (s, 1H), 8.05 (d, *J* = 15.6 Hz, 1H), 7.77-7.73 (m, 2H), 7.68 -7.57 (m, 1H), 6.92 (d, *J* = 8.2 Hz, 1H), 6.58 (s, 1H), 5.89 (dd, *J* = 16.7, 6.5 Hz, 1H), 5.23 (m, 1H), 4.93 (dd, *J* = 17.1, 1.7 Hz, 1H), 4.87 (d, *J* = 8.9 Hz, 1H), 4.65 (d, *J* = 6.4 Hz, 2H), 3.83 (s, 3H), 3.22 (d, *J* = 6.5 Hz, 2H), 1.80 (s, 3H), 1.68 (s, 3H). ^{13}C-NMR (125 MHz, acetone-d_6) δ (ppm): 188.4, 159.8, 159.4, 152.0, 148.5, 143.2, 139.3, 138.1, 132.1, 131.4, 123.9, 120.1, 120.3, 119.3, 115.6, 115.4, 115.3, 112.1, 99.8, 66.9, 56.5, 41.5 ×2, 34.1. ESI-MS *m/z*: 395.09 $(M+H)^+$, calcd for $C_{24}H_{26}O_5$: 394.18.

5.1.6.11 (*E*)-3-(5-Allyl-4-hydroxy-2-methoxyphenyl)-1-[4-(allyloxy)-2-methoxyphenyl]prop-2-en-1-one (13). Yellow solid, 56.3% yield, m.p: 120.7-122.8 °C. ^{1}H-NMR (500 MHz, acetone--d_6) δ ppm: 8.92 (s, 1H), 8.46 (s, 1H), 8.05 (d, *J* = 15.6 Hz, 1H), 7.76 -7.75 (m, 2H), 7.65-7.57 (m, 2H), 6.92 (d, *J* = 8.2 Hz, 1H), 6.58 (s, 1H), 5.89 (dd, *J* = 16.7, 6.5 Hz, 1H), 5.23 (m, 1H), 4.93 (dd, *J* = 17.1, 1.7 Hz, 1H), 4.87 (d, *J* = 8.9 Hz, 1H), 4.65 (d, J = 6.4 Hz, 2H), 3.91 (s, 3H), 3.83 (s, 3H), 3.22 (d, *J* = 6.5 Hz, 2H), 1.80 (s, 3H), 1.68 (s, 3H). ^{13}C-NMR (125 MHz, acetone-d_6) δ (ppm): 188.4, 159.8, 159.4, 152.0, 148.5, 139.3, 138.1, 132.1, 131.4, 123.9, 120.1, 119.4, 116.6, 115.3, 115.3,

112.1, 108.7, 106.3, 102.3, 99.8, 66.9, 56.5, 56.0, 34.1, 31.2. ESI-MS *m/z*: 409.24 $(M+H)^+$, calcd for $C_{25}H_{28}O_5$: 408.19.

5.1.6.12 (*E*)-3-(5-Allyl-4-hydroxy-2-methoxyphenyl)-1-(3-allyl-4-methoxyphenyl)prop-2-en-1-one (14). Yellow-green solid, 60.43% yield, m.p: 119.7-121.9 °C. ^{1}H-NMR (125 MHz, acetone-d_6) δ (ppm): 8.83 (s, 1H), 7.92 (d, *J* = 15.6 Hz, 1H), 7.87 (dd, *J* = 8.5, 2.1 Hz, 1H), 7.77 (s, 1H), 7.56 (d, *J* = 15.6 Hz, 1H), 7.44 (s, 1H), 6.92 (d, *J* = 8.6 Hz, 1H), 6.46 (s, 1H), 5.97-5.78 (m, 2H), 4.98-4.91 (m, 2H), 4.88 (dd, *J* = 16.6, 10.7 Hz, 2H), 3.77 (s, 3H), 3.72 (s, 3H), 3.23 (d, *J* = 5.8 Hz, 4H). ^{13}C-NMR (125 MHz, acetone-d_6) δ (ppm): 189.8, 161.7, 159.8, 159.5, 139.6, 138.0, 137.4, 132.4, 131.4, 130.8, 129.6, 129.4, 120.1, 119.6, 116.5, 116.1, 115.4, 110.8, 99.9, 56.1, 56.0, 34.8, 34.1. ESI-MS *m/z*: 366.06 $(M+H)^+$, calcd for $C_{23}H_{24}O_4$: 364.17.

5.1.6.13 (*E*)-3-(5-Allyl-4-hydroxy-2-methoxyphenyl)-1-[4-methoxy-3-(3-methylbut-3-en-2-yl)phenyl]prop-2-en-1-one (15). Yellow solid, 45.33% yield, m.p: 123.5-125.1 °C. ^{1}H-NMR (500 MHz, acetone-d_6) δ (ppm): 8.90 (s, 1H), 7.88 (d, *J* = 8.6 Hz, 2H), 7.87 (dd, *J* = 8.5, 2.1 Hz, 1H), 7.77 (s, 1H), 7.56 (d, *J* = 15.6 Hz, 1H), 7.44 (s, 1H), 6.92 (d, *J* = 8.6 Hz, 1H), 6.46 (s, 1H), 5.90 (dd, *J* = 16.7, 6.5 Hz, 1H), 4.98-4.91 (m, 2H), 4.88 (dd, *J* = 16.6, 10.7 Hz, 2H), 3.77 (s, 3H), 3.72 (s, 3H), 3.23 (d, *J* = 5.8 Hz, 2H), 1.82 (s, 3H), 1.75 (s, 3H). ^{13}C-NMR (125 MHz, acetone-d_6) δ (ppm): 189.7, 161.7, 159.8, 159.3, 149.00, 139.4, 138.0, 137.2, 132.4, 131.4, 130.8, 129.7, 120.1, 119.6, 116.4, 116.1, 115.4, 111.2, 99.9, 56.2, 56.0, 34.3, 34.1, 21.2, 20.1. ESI-MS *m/z*: 393.34 $(M+H)^+$, calcd for $C_{25}H_{28}O_4$: 392.20.

5.1.6.14 (*E*)-3-(5-Allyl-4-hydroxy-2-methoxyphenyl)-1-[4-methoxy-3-(3-methylbut-2-en-1-yl)phenyl]prop-2-en-1-one (16). Yellow solid, 34.33% yield, m.p: 139.2-141.5 °C. ^{1}H-NMR (500

MHz, acetone-d_6) δ (ppm): 8.79 (s, 1H), 7.89 (d, *J* = 8.5 Hz, 2H), 7.85 (dd, *J* = 8.4, 2.6 Hz, 1H), 7.74 (s, 1H), 7.56 (d, *J* = 15.6 Hz, 1H), 7.41 (s, 1H), 6.91 (d, *J* = 8.5 Hz, 1H), 6.48 (s, 1H), 5.90 (dd, *J* = 16.7, 6.5 Hz, 1H), 5.78 (s, 1H) 4.98-4.91 (m, 2H), 4.88 (dd, *J* = 16.6, 10.7 Hz, 2H), 3.77 (s, 3H), 3.72 (s, 3H), 3.23 (d, *J* = 5.8 Hz, 2H), 1.85 (s, 3H), 1.72 (s, 3H). ^{13}C-NMR (125 MHz, acetone-d_6) δ (ppm): 189.6, 162.5, 159.4, 140.7, 138.4, 138.0, 132.4, 131.4, 130.8, 129.7, 121.6, 120.1, 119.6, 116.3, 116.1, 114.4, 111.1, 99.9, 56.2, 56.0, 34.3, 34.1, 25.3, 20.1, 14.6. ESI-MS *m/z*: 393.13 $(M+H)^+$, calcd for $C_{25}H_{28}O_4$: 392.20.

5.1.6.15 (*E*)-3-(5-Allyl-4-hydroxy-2-methoxyphenyl)-1-[4-(piperidin-1-yl)phenyl]prop-2-en-1-one (17). Yellow solid, 36.97% yield, m.p: 179.1-181.2 °C. ^{1}H NMR (500 MHz, DMSO-d_6) δ (ppm): 10.12 (s, 1H), 7.97 (d, *J* = 8.8 Hz, 2H), 7.91 (d, *J* = 15.6 Hz, 1H), 7.64 (d, *J* = 6.0 Hz, 1H), 7.62 (s, 1H), 6.99 (d, *J* = 7.8 Hz, 2H), 6.54 (s, 1H), 5.90 (dd, *J* = 16.7, 6.5 Hz, 1H), 4.93 (dd, *J* = 17.1, 1.7 Hz, 1H), 4.87 (d, *J* = 8.9 Hz, 1H), 3.82 (s, 3H), 3.40 (d, *J* = 19.4 Hz, 4H), 3.22 (d, *J* = 6.5 Hz, 2H), 1.62-1.33 (m, 6H). ^{13}C-NMR (125 MHz, DMSO-d_6) δ (ppm): 186.4, 159.4, 158.2, 153.5, 137.2 ×2, 137.2, 130.2, 129.9 ×2, 119.9, 118.0, 114.9 ×2, 114.4, 113.1, 99.8, 65.0, 55.5 ×2, 47.9, 33.1, 24.9, 23.8. ESI-MS *m/z*: 378.31 $(M+H)^+$, calcd for $C_{24}H_{27}NO_3$: 377.20.

5.1.6.16 (*E*)-3-(5-Allyl-4-hydroxy-2-methoxyphenyl)-1-[2-(piperidin-1-yl)phenyl]prop-2-en-1-one (18). Yellow solid, 29.34% yield, m.p: 175.3-177.1 °C. ^{1}H-NMR (500 MHz, acetone--d_6) δ (ppm): 9.00 (s, 1H), 7.83 (d, *J* = 16.0 Hz, 1H), 7.60 (d, *J* = 2.4 Hz, 1H), 7.50 (d, *J* = 3.2 Hz, 1H), 7.41 (d, *J* = 17.0 Hz, 1 H), 7.28 (d, *J* = 28.6 Hz, 1H), 7.01 (s, 1H), 6.89 (s, 1H), 6.49 (s, 1H), 5.90 (dd, *J* = 16.7, 6.5 Hz, 1H), 4.92 (dd, *J* = 17.1, 1.7 Hz, 1H), 4.87 (d, *J* = 8.9 Hz, 1H), 3.74 (s, 3H), 3.22 (d, *J* = 6.5 Hz, 2H), 2.88 (d, *J* = 2.1 Hz, 4H), 1.64-1.48 (m, 6H), ^{13}C-NMR (125 MHz, DMSO-d_6) δ (ppm): 193.4, 167.9, 159.6, 136.7, 133.4, 132.4, 131.9, 130.3, 129.5 ×2, 120.2, 116.3, 115.5,

99.9, 66.8, 56.0 ×2, 55.2, 34.0, 32.6, 31.3, 26.9, 24.7, 23.3. ESI-MS *m/z*: 378.41 $(M+H)^+$, calcd for $C_{24}H_{27}NO_3$: 377.20.

5.1.6.17 (*E*)-3-(5-Allyl-4-hydroxy-2-methoxyphenyl)-1-[3-(piperidin-1-yl)phenyl]prop-2-en-1-one (19). Yellow solid, 45.89% yield, m.p: 178.3 -179.8 °C. ^{1}H NMR (500 MHz, acetone-d_6) δ (ppm): 9.03 (s, 1H), 7.88 (d, *J* = 16.0 Hz, 1H), 7.61 (d, *J* = 2.4 Hz, 1H), 7.51 (d, *J* = 3.2 Hz, 1H), 7.41 (d, *J* = 17.0 Hz, 1 H), 7.33 (d, *J* = 18.6 Hz, 1H), 7.01 (s, 1H), 6.91 (s, 1H), 6.51 (s, 1H), 5.90 (dd, *J* = 16.7, 6.5 Hz, 1H), 4.93 (dd, *J* = 17.1, 1.7 Hz, 1H), 4.87 (d, *J* = 8.9 Hz, 1H), 3.71 (s, 3H), 3.22 (d, *J* = 6.5 Hz, 2H), 2.88 (d, *J* = 2.1 Hz, 4H), 1.64-1.48 (m, 6H). ^{13}C-NMR (125 MHz, DMSO-d_6) δ (ppm): 194.6, 167.9, 159.6, 133.4, 132.5, 131.9, 130.3, 129.6, 128.5, 120.2, 116.4, 115.5, 114.4, 99.9, 66.9, 56.0, 55.1 ×2, 34.0, 32.6, 31.3, 26.9, 24.7, 23.3. ESI-MS *m/z*: 378.18 $(M+H)^+$, calcd for $C_{24}H_{27}NO_3$: 377.20.

5.1.6.18 (*E*)-3-(5-Allyl-4-hydroxy-2-methoxyphenyl)-1-(4-morpholinophenyl)prop-2-en-1-one (20). Yellow solid, 45.84% yield, m.p: 163.7-165.0 °C. ^{1}H-NMR (500 MHz, DMSO--d_6) δ (ppm): 10.13 (s, 1H), 8.01 (d, *J* = 8.8 Hz, 2H), 7.92 (d, *J* = 15.6 Hz, 1H), 7.72 (s, 1H), 7.66 (d, *J* = 4.6 Hz, 1H), 7.02 (d, *J* = 8.8 Hz, 2H), 6.53 (s, 1H), 5.90 (dd, *J* = 16.7, 6.5 Hz, 1H), 4.93 (dd, *J* = 17.1, 1.7 Hz, 1H), 4.87 (d, *J* = 8.9 Hz, 1H), 3.82 (s, 3H), 3.77-3.70 (m, 4H), 3.32-3.29 (m, 4H), 3.22 (d, *J* = 6.5 Hz, 2H), ^{13}C-NMR (125 MHz, DMSO-d_6) δ (ppm): 186.5, 159.8, 158.2, 153.7, 137.4, 131.4, 130.1, 129.9, 128.2, 118.9, 117.9, 114.9, 113.3, 112.9, 98.8, 66.8, 64.9, 56.5, 46.8, 33.1, 29.9, 19.6, 13.4. ESI-MS *m/z*: 380.20 $(M+H)^+$, calcd for $C_{23}H_{25}NO_4$: 379.18.

5.1.6.19 (*E*)-1-[4-(*1H*-pyrazol-1-yl)phenyl]-3-(5-allyl-4-hydroxy-2-methoxyphenyl)prop-2-en-1-one (21). Brownish yellow solid, 42.1% yield, m.p: 135.4-137.6 °C. ^{1}H NMR (500 MHz, acetone-d_6)

δ (ppm): 8.78 (s, 1H), 7.89 (d, *J* = 8.5 Hz, 2H), 7.85 (dd, *J* = 8.7, 2.6 Hz, 1H), 7.78 (s, 1H), 7.56 (d, *J* = 15.6 Hz, 1H), 7.41 (s, 1H), 7.29 (d, *J* = 8.5 Hz, 2H), 6.92 (d, *J* = 8.2 Hz, 1H), 6.91 (d, *J* = 8.5 Hz, 1H), 6.48 (s, 1H), 5.90 (dd, *J* = 16.7, 6.5 Hz, 1H), 4.93 (dd, *J* = 17.1, 1.7 Hz, 1H), 4.87 (d, *J* = 8.9 Hz, 1H), 3.72 (s, 3H), 3.22 (d, *J* = 6.5 Hz, 2H), ^{13}C-NMR (125 MHz, acetone-d_6) δ (ppm): 188.79, 167.25, 160.21, 159.57, 158.42, 155.35, 140.34, 138.99, 134.57, 131.89, 130.43, 130.16, 129.63, 122.94, 119.68, 119.27, 116.22, 115.42, 109.35, 99.89, 56.03, 34.13. ESI-MS *m/z*: 362.30 $(M+H)^+$, calcd for $C_{22}H_{20}N_2O_3$: 360.15.

5.1.6.20 (*E*)-3-(5-Allyl-4-hydroxy-2-methoxyphenyl)-1-[4-(dimethylamino)phenyl]prop-2-en-1-one (22). Yellow solid, 48.3% yield, m.p: 151.6-153.1 °C. ^{1}H-NMR (500 MHz, acetone-d_6) δ (ppm): 8.91 (s, 1H), 8.03 (dd, *J* = 12.1, 9.5 Hz, 3H), 7.71 (d, *J* = 15.6 Hz, 1H), 7.61 (s, 1H), 6.80 (d, *J* = 8.9 Hz), 6.61 (s, 1H), 6.04 (dt, *J* = 16.7, 8.3 Hz), 5.09 (d, *J* = 17.1 Hz, 1H), 5.02 (d, *J* = 10.0 Hz, 1H), 3.88 (s, 3H), 3.38 (d, *J* = 6.3 Hz, 2H), 3.10 (s, 6H). ^{13}C-NMR (125 MHz, acetone-d_6) δ (ppm): 189.1, 168.7, 168.3, 142.5, 141.2, 139.4, 135.4, 129.7, 129.4, 127.2, 122.1, 118.4, 118.2, 115.9, 113.3, 113.1, 97.0, 64.0, 53.6, 44.2, 31.7. ESI-MS *m/z*: 338.34 $(M+H)^+$, calcd for $C_{21}H_{23}NO_3$: 337.17.

5.1.6.21 (*E*)-3-(5-Allyl-4-hydroxy-2-methoxyphenyl)-1-[3-(dimethylamino)phenyl]prop-2-en-1-one (23). Yellow solid, 59.36% yield, m.p: 159.8-162.8 °C. ^{1}H NMR (500 MHz, $CDCl_3$) δ (ppm): 8.91 (s, 1H), 8.05 (s, 1H), 8.03 (d, *J* = 2.6 Hz, 1H), 8.01 (d, *J* = 6.4 Hz, 1H), 7.71 (d, *J* = 15.6 Hz, 1H), 7.61 (s, 1H), 6.80 (d, *J* = 8.9 Hz, 2H), 6.61 (s, 1H), 5.90 (dd, *J* = 16.7, 6.5 Hz, 1H), 4.93 (dd, *J* = 17.1, 1.7 Hz, 1H), 4.87 (d, *J* = 8.9 Hz, 1H), 3.88 (s, 3H), 3.22 (d, *J* = 6.5 Hz, 2H), 3.10 (s, 6H). ^{13}C-NMR (125 MHz, acetone-d_6) δ (ppm): 188.2, 168.7, 168.3, 142.5, 141.0, 139.4, 135.6, 129.7, 129.4, 127.1, 122.1, 118.4, 118.2, 115.9, 113.4, 113.9, 97.0, 64.0, 53.7, 44.2, 31.7. ESI-MS *m/z*: 339.01 $(M+H)^+$, calcd for $C_{21}H_{23}NO_3$: 337.17.

5.1.6.22 (*E*)-3-(5-Allyl-4-hydroxy-2-methoxyphenyl)-1-[2-(dimethylamino)phenyl]prop-2-en-1-one (24). Yellow solid, 60.15% yield, m.p: 148.6-150.2 °C. ^{1}H-NMR (500 MHz, $CDCl_3$) δ (ppm): 8.87 (s, 1H), 8.05 (d, *J* = 5.4 Hz, 1H), 8.03 (d, *J* = 2.6 Hz, 2H), 7.99 (d, *J* = 6.4 Hz, 1H), 7.77 (d, *J* = 15.6 Hz, 1H), 7.61 (s, 1H), 6.80 (d, *J* = 8.9 Hz, 1H), 6.58 (s, 1H), 5.90 (dd, *J* = 16.7 Hz, 10.1, 6.5 Hz, 1H), 4.93 (dd, *J* = 17.1, 1.7 Hz, 1H), 4.87 (d, *J* = 8.9 Hz, 1H), 3.88 (s, 3H), 3.22 (d, *J* = 6.5 Hz, 2H), 3.10 (s, 6H). ^{13}C-NMR (125 MHz, acetone-d_6) δ (ppm): 188.4, 169.4, 167.3, 142.3, 141.0, 138.6, 134.6, 129.6, 128.3, 126.2, 122.1, 118.5, 118.2, 115.9, 113.4, 113.9, 97.0, 63.2, 53.8, 44.2, 31.7. ESI-MS *m/z*: 338.22 $(M+H)^+$, calcd for $C_{21}H_{23}NO_3$: 337.17.

5.1.6.23 (*E*)-3-(5-Allyl-4-hydroxy-2-methoxyphenyl)-1-[3-(dimethylamino)phenyl]prop-2-en-1-one (25). Yellow solid, 59.36% yield, m.p: 167.3-169.5 °C. ^{1}H-NMR (500 MHz, $CDCl_3$) δ (ppm): 8.89 (s, 1H), 8.04 (s, 1H), 8.03 (d, *J* = 2.6 Hz, 1H), 8.01 (d, *J* = 6.4 Hz, 1H), 7.71 (d, *J* = 15.6 Hz, 1H), 7.66 (d, *J* = 4.6 Hz, 2H), 7.61 (s, 1H), 7.02 (d, *J* = 8.8 Hz, 2H), 6.92 (d, *J* = 8.2 Hz, 1H), 6.80 (d, *J* = 8.9 Hz, 2H), 6.61 (s, 1H), 5.90 (dd, *J* = 16.7, 6.5 Hz), 4.93 (dd, *J* = 17.1, 1.7 Hz, 1H), 4.87 (d, *J* = 8.9 Hz, 1H), 3.82 (s, 3H), 2.88 (s, 6H). ^{13}C-NMR (125 MHz, acetone-d_6) δ (ppm): 189.3, 160.6, 159.5, 157.7, 140.1, 134.3, 130.1 ×2, 129.7, 128.2, 121.6, 121.3, 120.3, 115.9, 112.4, 107.4, 101.4, 99.9, 72.5, 45.9, 34.1. ESI-MS *m/z*: 414.02 $(M+H)^+$, calcd for $C_{27}H_{27}NO_3$: 413.20.

5.1.6.24 (*E*)-3-(5-Allyl-4-hydroxy-2-isopropoxyphenyl)-1-[3-(dimethylamino)phenyl]prop-2-en-1-one (26). Yellow solid, 48.98% yield, m.p: 137.4-139.6 °C. ^{1}H-NMR (500 MHz, acetone--d_6) δ (ppm): 8.79 (s, 1H), 8.05 (d, *J* = 15.7 Hz, 1H), 7.92 (d, *J* = 15.6 Hz, 1H), 7.83 (d, *J* = 16.0 Hz, 2H), 7.76 (s, 1H), 7.53 (d, *J* = 4.9 Hz, 1H), 7.48 (s, 1H), 7.41 (d, *J* = 17.0 Hz, 1H), 6.45 (s, 1H), 5.90 (dd, *J* = 16.7, 6.5 Hz, 1H), 4.93 (dd, *J* = 17.1, 1.7 Hz, 1H), 4.87 (d, *J* = 8.9 Hz, 1H), 3.82 (s, 3H), 2.88 (s,

6H), 1.72 (s, 6H). ^{13}C-NMR (125 MHz, acetone-d_6) δ (ppm): 188.8, 159.2, 152.6, 151.3, 142.4, 138.7, 136.5, 134.2, 128.9, 121.4, 121.3, 120.9, 120.1, 118.3, 115.9, 109.8, 102.1, 99.8, 75.4, 44.3, 34.1, 23.1 ×2. ESI-MS *m/z*: 366.25 $(M+H)^+$, calcd for: $C_{23}H_{27}NO_3$: 365.20.

5.1.6.25 (*E*)-*N*-{3-[3-(5-Allyl-4-hydroxy-2-methoxyphenyl)acryloyl]phenyl}methanesulfonamide (27). Yellow solid, 45.92% yield, m.p: 167.4-169.8 °C. ^{1}H-NMR (500 MHz, acetone-d_6) δ (ppm): 9.06 (s, 1H), 8.79 (s, 1H), 8.05 (d, *J* = 15.7 Hz, 1H), 7.98 (s, 1H), 7.83 (d, *J* = 7.6 Hz, 1H), 7.63 (d, *J* = 15.7 Hz, 1H), 7.63 (d, *J* = 15.7 Hz, 1H), 7.57 (d, *J* = 7.9 Hz, 2H), 7.51 (d, *J* = 7.8 Hz, 1H), 6.59 (s, 1H), 5.90 (dd, *J* = 16.7, 6.5 Hz, 1H), 4.93 (dd, *J* = 17.1, 1.7 Hz, 1H), 4.87 (d, *J* = 8.9 Hz, 1H), 3.85 (s, 3H), 3.22 (d, *J* = 6.5 Hz, 2H), 3.03 (s, 3H). ^{13}C-NMR (125 MHz, acetone-d_6) δ (ppm): 189.9, 160.1, 159.9, 141.1, 141.0, 139.9, 137.9, 131.9, 130.5, 124.9, 124.6, 120.5, 120.3, 119.5, 116.3, 115.5, 99.9, 56.0, 39.6, 34.1. ESI-MS *m/z*: 388.07 $(M+H)^+$, calcd for $C_{20}H_{21}NO_5S$: 387.11.

5.1.6.26 (*E*)-3-(5-Allyl-4-hydroxy-2-methoxyphenyl)-1-[6-(dimethylamino)benzo[d][1,3]dioxol-5-yl]prop-2-en-1-one (28). Yellow solid, 49.76% yield, m.p: 159.3-162.1 °C. ^{1}H-NMR (500 MHz, acetone-d_6) δ (ppm): 8.99 (s, 1H), 8.05 (d, *J* = 15.6 Hz, 1H), 7.83 (s, 1H), 7.63 (s, 1H), 7.56 (d, *J* = 15.6 Hz, 1H), 7.41 (s, 1 H), 6.49 (s, 1H), 6.03 (s, 2H) 5.90 (dd, *J* = 16.7, 6.5 Hz, 1H), 4.93 (dd, *J* = 17.1, 1.7 Hz, 1H), 4.87 (d, *J* = 8.9 Hz, 1H), 3.72 (s, 3H), 3.20 (dd, *J* = 14.2, 6.5 Hz, 2H), 3.02 (s, 6H). ^{13}C-NMR (125 MHz, acetone-d_6) δ (ppm): 186.4, 158.3, 158.0, 150.2, 144.1, 138.3, 136.7, 130.3, 129.8, 129.0, 121.5, 121.0, 121.0, 115.2, 113.4, 113.2, 110.6, 101.2, 99.4, 54.9, 32.7. ESI-MS *m/z*: 382.60 $(M+H)^+$, calcd for $C_{22}H_{23}NO_5$: 381.16.

5.1.6.27 (*E*)-3-(5-Allyl-4-hydroxy-2-methoxyphenyl)-1-[3-(diallylamino)phenyl]prop-2-en-1-one

(29). Yellow solid, 59.36% yield, m.p: 145.7-147.3 °C. ^{1}H-NMR (500 MHz, acetone-d_6) δ (ppm): 8.90 (s, 1H), 7.90 (d, *J* = 15.6 Hz, 1H), 7.46 (d, *J* = 15.7 Hz, 1H), 7.42 (d, *J* = 14.2 Hz, 1H), 7.23 (s, 1H), 7.19 (d, *J* = 7.5 Hz, 1H), 7.16 (d, *J* = 7.9 Hz, 1H), 6.80 (dd, *J* = 7.9, 1.8 Hz, 1H), 6.47 (s, 1H), 5.90 (dd, *J* = 16.7, 6.5 Hz, 1H), 5.84-5.71 (m, 2H), 5.13-4.99 (m, 4H), 4.93 (dd, *J* = 17.1, 1.7 Hz, 1H), 4.87 (d, *J* = 8.9 Hz, 1H), 3.90 (d, *J* = 4.5 Hz, 4H), 3.73 (s, 3H), 3.21 (dd, *J* = 14.0, 6.6 Hz, 2H). ^{13}C-NMR (125 MHz, acetone-d_6) δ (ppm): 190.9, 187.3, 163.5, 159.9, 159.6, 149.69, 140.6, 140.0, 139.0, 135.0, 131.5, 130.3, 129.9, 120.2, 117.0, 116.4, 116.3, 115.8, 115.4, 112.5, 99.8, 99.4, 56.0, 53.6, 34.1. ESI-MS *m/z*: 391.19 $(M+H)^+$, calcd for $C_{25}H_{27}NO_3$: 389.20.

5.1.6.28 (*E*)-3-(5-Allyl-4-hydroxy-2-methoxyphenyl)-1-[4-(diallylamino)phenyl]prop-2-en-1-one (30). Yellow solid, 62.50% yield, m.p: 141.2-142.9 °C. ^{1}H NMR (500 MHz, acetone--d_6) δ (ppm): 8.90 (s, 1H), 7.90 (d, *J* = 15.7 Hz, 1H), 7.46 (d, *J* = 15.7 Hz, 1H), 7.41 (d, *J* = 11.3 Hz, 1H), 7.23 (s, 1H), 7.19 (d, *J* = 7.5 Hz, 1H), 7.16 (d, *J* = 7.9 Hz, 1H), 6.80 (dd, *J* = 7.8, 1.6 Hz, 1H), 6.47 (s, 1H), 5.90 (dd, *J* = 16.7, 6.5 Hz, 1H), 5.84-5.71 (m, 2H), 5.13-4.99 (m, 4H), 4.93 (dd, *J* = 17.1, 1.7 Hz, 1H), 4.87 (d, *J* = 8.9 Hz, 1H), 3.90 (d, *J* = 4.5 Hz, 4H), 3.72 (s, 3H), 3.20 (dd, *J* = 14.2, 6.5 Hz, 2H). ^{13}C-NMR (125 MHz, acetone-d_6) δ (ppm): 191.9, 187.4, 159.9, 159.6, 149.6, 140.6, 138.0, 135.0 ×2, 131.5, 130.3, 129.9, 120.2, 117.0, 116.4, 116.3, 115.8, 115.4, 112.5, 99.4, 99.4, 56.0, 53.6, 53.1, 34.1. ESI-MS *m/z*: 390.29 $(M+H)^+$, calcd for $C_{25}H_{27}NO_3$: 389.20.

5.1.8 Synthesis of 5-allyl-2-methoxy-4-[(tetrahydro-2H-pyran-2-yl)oxy]benzaldehyde (6a). A solution of 5-allyl-4-hydroxy-2-methoxybenzaldehyde **3a** (1.2 g, 6.25 mmol) in dry CH_2Cl_2 (15 mL) was added 3,4-dihydro-2H-pyran (0.86 g, 10.28 mmol) portionwise, followed by PPTS (67 mg, 0.21 mmol). The reaction mixture was stirred overnight at 40 ^{o}C.The resulting solution was quenched with redistilled water (20 mL) and extracted with EtOAc (3 × 20 mL). The combined organic layers

were washed with water (500 mL), brine (500 mL), dried over anhydrous $MgSO_4$, and concentrated under reduced pressure. The residue was purified by chromatography on silica gel provided desired compound **6a** (1.38 g, 80%) as a colorless liquid. ^{1}H-NMR (500 MHz, DMSO-d_6) δ (ppm): 10.27 (S, 1H), 7.62 (S, 1H), 7.28 (S, 1H), 6.73-6.45 (m, 1H), 5.99-5.91 (m, 1H), 5.18-5.06 (m, 2H), 3.86 (s, 3H), 3.66-3.52 (m, 2H), 3.35 (d. *J* = 5.0 Hz, 2H), 2.00-1.54 (m, 6H).

5.1.7 Synthesis of Compounds 2 and 9. The synthetic procedure of Compounds **2** and **9** from Compound **6a** was identical with that of compounds **5a** described above.

5.1.7.1 (*E*)-3-{5-Allyl-2-methoxy-4-[(tetrahydro-2H-pyran-2-yl)oxy]phenyl}-1-(4-hydroxyphenyl)prop-2-en-1-one (2) Yellow liquid, 45.3% yield, ^{1}H NMR (500 MHz, acetone--d_6) δ (ppm): 8.98 (s, 1H), 8.71 (s, 1H), 7.90 (d, *J* = 15.7 Hz, 1H), 7.88 (d, *J* = 8.6 Hz, 2H), 7.50 (d, *J* = 15.6 Hz, 1H), 7.47 (s, 1H), 6.8 (d, *J* = 8.5 Hz, 1H), 6.47 (s, 1H), 5.90 (ddt, *J* = 16.7, 10.1, 6.5 Hz, 1H), 5.76 (m, 1H), 4.93 (dd, *J* = 17.1, 1.7 Hz, 1H), 4.87 (d, *J* = 8.9 Hz, 1H), 3.74 (s, 3H), 3.60 (t, *J* = 8.6 Hz, 2H), 3.22 (d, *J* = 6.5 Hz, 2H), 2.22 (m, 2H), 1.93 (m, 2H), 1.71 (m, 2H). ^{13}C-NMR (125 MHz, acetone--d_6) δ (ppm): 188.4, 162.3, 159.7, 159.2, 139.2, 138.1, 131.7, 131.5 ×2, 131.4, 120.1, 119.5, 116.6, 116.0 ×2, 102.3, 115.4, 99.9, 62.4, 56.0, 34.2, 30.4, 24.6, 20.4. ESI-MS *m/z*: 395.26 $(M+H)^+$, calcd for $C_{24}H_{26}O_5$: 394.18.

5.1.7.2 (*E*)-3-{5-Allyl-2-methoxy-4-[(tetrahydro-2H-pyran-2-yl)oxy]phenyl}-1-[4-(allyloxy)-2-hydroxyphenyl]prop-2-en-1-one (9) Yellow liquid, 49.78% yield, ^{1}H-NMR (500 MHz, acetone--d_6) δ (ppm): 8.05 (d, *J* = 15.6 Hz, 1H), 7.90 (d, *J* = 9.4 Hz, 1H), 7.63 (dd, *J* = 9.7, 5.8 Hz, 1H), 7.53 (s, 1H), 6.50 (s, 1H), 6.41 (d, *J* = 15.6 Hz, 1H), 6.33 (s, 1H), 6.01-5.80 (m, 2H), 5.76 (m, 1H), 5.30 (d, *J* = 17.2 Hz, 1H), 5.15 (d, *J* = 9.1 Hz, 1H), 4.93 (dd, *J* = 17.1, 1.7 Hz, 1H), 4.87 (d, *J* = 8.9 Hz, 1H),

4.53 (d, *J* = 4.4 Hz, 2H), 3.73 (s, 3H), 3.60 (t, *J* = 8.6 Hz, 2H), 3.22 (d, *J* = 6.5 Hz, 2H), 2.43 (m, 2H), 1.9 3 (m, 2H), 1.69 (m, 2H). ^{13}C-NMR (125 MHz, acetone--d_6) δ (ppm): 188.5, 163.0, 159.5, 139.7, 138.0, 134.2, 133.7, 131.9, 131.4, 131.3, 129.6, 120.2, 119.4, 117.8, 116.6, 115.5, 115.3, 103.3, 99.9, 69.3, 66.9, 63.2, 56.0, 34.1, 30.2, 24.8, 20.72. ESI-MS *m/z*: 451.37 $(M+H)^+$, calcd for $C_{27}H_{30}O_6$: 450.20.

5.1.8 Synthesis of (*E*)-3-[5-allyl-2-methoxy-4-(methoxymethoxy)phenyl]-1-{4-[2-(trimethylsilyl) ethoxy]methoxy}prop-2-en-1-one (7a). The synthetic procedure for **7a** from Compound **4a** was identical with that of Compound **5a** described above. **7a**: yield 85.0%, as a yellow oil. ^{1}H-NMR (500 MHz, DMSO-d_6) δ (ppm): 8.15 (d, *J* = 8.6 Hz, 2H), 8.02 (d, *J* = 15.6 Hz, 1H), 7.86-7.75 (m, 2H), 7.18 (d, *J* = 8.6 Hz, 2H), 7.18 (d, *J* = 8.6 Hz, 1H), 6.03 (ddd, *J* = 13.2, 12.7, 6.3 Hz, 1H), 5.37 (s, 2H), 5.07 (d, *J* = 17.3 Hz, 2H), 3.92 (s, 3H), 3.80-3.68 (m, 2H), 3.45 (s, 3H), 3.37 (d, *J* = 6.0 Hz, 2H), 0.95-0.91 (m, 2H), 0..05 (s, 9H). ESI-MS *m/z*: 484.86 $(M+H)^+$, calcd for $C_{27}H_{36}O6Si$: 484.23.

5.1.9 Synthesis of (*E*)-3-[5-allyl-2-methoxy-4-(methoxymethoxy)phenyl]-1-(4-hydroxyphenyl)prop-2-en-1-one (8a). Et_3N (4.8 g, 80.97 mmol) was added portionwise to a solution of **7a** (2.6 g, 5.4 mmol) in THF (30 mL), followed by tetrabutylammonium fluoride (21.0 g, 80.97 mmol) added dropwise. The reaction mixture was refluxed at 65 °C for 20 min. The reaction mixture was quenched with water (30 mL) and concentrated under reduced pressure. The mixture was then extracted with EtOAc (3 × 30 mL). The combined organic layers were washed with brine (50 mL), dried over $MgSO_4$, and concentrated under reduced pressure. The residue was further purified by chromatography on silica gel to obtain Compound **8a** (5.24 g, 80%) as a yellow solid. ^{1}H-NMR (500 MHz, acetone-d_6) δ (ppm): 8.08 (t, *J* = 2.1 Hz, 2H), 8.06-8.05 (m, 1H), 7.80-7.75 (m, 1H), 7.71 (s, 1H), 7.00 (d, *J* = 2.0 Hz, 1H), 6.98 (d, *J* = 2.0 Hz, 1H), 6.89 (s, 1H), 6.05 (ddt, *J* = 16.6,

10.0, 6.5 Hz, 1H), 5.37 (s, 1H), 5.09 (ddd, *J* = 17.1, 3.6, 1.6 Hz, 1H), 5.03 (ddd, *J* = 10.0, 3.4, 1.3 Hz, 1H), 3.97 (s, 3H), 3.51 (s, 3H), 3.40 (d, *J* = 6.4 Hz, 2H). ESI-MS *m/z*: 355.28 $(M+H)^+$, $C_{21}H_{22}O_5$: 354.15.

5.1.10 Synthesis of compounds 31-33. Different benzoyl chlorides (0.85 mmol), followed by Et_3N (0.15 mL, 1.2 mmol), was added dropwise to a solution of **8a** (100 mg, 0.28 mmol) in THF (10 mL). The reaction mixture was stirred at room temperature for 8 h. The resulting mixture was quenched with water (20 mL) and extracted with EtOAc (3× 30 mL). The combined organic layers were washed with brine (50 mL), dried over $MgSO_4$, and concentrated under reduced pressure. The residue was further dissolved in MeOH and H_2O (15 mL, v/v 2:1), and 6N-HCl was added dropwise to the solution. The reaction mixture was stirred at room temperature for 3-5 h, quenched with saturated aqueous NH_4Cl solution (20 mL) and extracted with EtOAc (3 × 20 mL). The combined organic layers were washed with brine (50 mL), dried over $MgSO_4$, filtered, and concentrated under reduced pressure. The residue was purified by chromatography on silica gel to obtain target compounds **31-33**, with 48.1-78% yields.

5.1.10.1 (*E*)-4-[3-(5-Allyl-4-hydroxy-2-methoxyphenyl)acryloyl]phenyl 4-(*tert*-butyl)benzoate (31). Yellow solid, 78% yield, m.p: 170.2-172.9 °C. ^{1}H-NMR (500 MHz, acetone-d_6) δ (ppm): 8.95 (s, 1H), 8.06 (d, *J* = 8.5 Hz, 2H), 8.04-7.98 (m, 2H), 7.98 (s, 1H), 7.65-7.58 (m, 1H), 7.53 (d, *J* = 4.9 Hz, 3H), 7.32 (d, *J* = 8.5 Hz, 2H), 6.48 (s, 1H), 5.95-5.83 (m, 1H), 4.93 (dd, *J* = 17.1, 1.7 Hz, 1H), 4.87 (d, *J* = 8.9 Hz, 1H), 3.75 (s, 3H), 3.23 (d, *J* = 5.8 Hz, 2H), 1.24 (s, 9H). ^{13}C-NMR (125 MHz, acetone-d_6) δ (ppm): 189.1, 165.1, 160.1, 159.8, 158.5, 155.3, 140.6, 138.0, 137.4, 134.80, 131.9, 131.6, 130.8, 130.6, 129.7, 129.6, 127.5, 126.6, 122.9, 120.3, 119.3, 116.3, 115.4, 99.8, 56.0, 35.8, 34.1, 31.3 ×3. ESI-MS *m/z*: 470.93 $(M+H)^+$, calcd for $C_{30}H_{30}O_5$: 470.21.

5.1.10.2 (*E*)-4-[3-(5-Allyl-4-hydroxy-2-methoxyphenyl)acryloyl]phenyl benzoate (32). Yellow solid 48.1% yield, m.p: 150.8 -152.4 °C. ^{1}H-NMR (500 MHz, acetone-d_6) δ (ppm): 8.95 (s, 1H), 8.05 (d, *J* = 8.5 Hz, 2HH), 8.04-7.98 (m, 3H), 7.98 (s, 1H), 7.63-7.58 (m, 1H), 7.51 (d, *J* = 4.9 Hz, 3H), 7.29 (d, *J* = 8.5 Hz, 2H), 6.48 (s, 1H), 5.90 (dd, *J* = 16.7, 6.5 Hz, 1H), 4.93 (dd, *J* = 17.1, 1.7 Hz, 1H), 4.87 (d, *J* = 8.9 Hz, 1H), 3.75 (s, 3H), 3.23 (d, *J* = 5.8 Hz, 2H). ^{13}C-NMR (125 MHz, acetone-d_6) δ (ppm): 189.1, 165.0, 160.1, 159.7, 158.4, 155.3, 140.5, 138.0, 137.9, 134.6, 131.9, 131.6, 130.8, 130.6, 129.6, 127.5, 122.9, 120.3, 119.3, 116.3, 115.4, 99.8, 56.0, 35.8, 34.1. ESI-MS *m/z*: 415.21 $(M+H)^+$, calcd for $C_{26}H_{22}O_5$: 414.15.

5.1.10.3 (*E*)-4-[3-(5-Allyl-4-hydroxy-2-methoxyphenyl)acryloyl]phenyl 4-bromobenzoate (33). Yellow solid, 64% yield, m.p: 173.1-175.2 °C. ^{1}H-NMR (500 MHz, acetone-d_6) δ (ppm): 8.92 (s, 1H), 8.00 (d, *J* = 8.5 Hz, 2H), 7.98.04-7.95 (m, 2H), 7.94 (s, 1H), 7.63-7.58 (m, 1H), 7.51 (d, *J* = 4.9 Hz, 3H), 7.25 (d, *J* = 8.5 Hz, 2H), 6.44 (s, 1H), 5.90 (dd, *J* = 16.7, 6.5 Hz, 1H), 4.93 (dd, *J* = 17.1, 1.7 Hz, 1H), 4.87 (d, *J* = 8.9 Hz, 1H), 3.73 (s, 3H), 3.22 (d, *J* = 5.8 Hz, 2H), ^{13}C-NMR (125 MHz, acetone-d_6) δ (ppm): 188.8, 165.2, 160.1, 159.7, 158.4, 155.3, 140.4, 138.0, 137.9, 134.5, 131.8, 131.6, 130.4, 130.1, 129.6, 127.5, 122.9, 119.6, 119.3, 116.2, 115.4, 99.8, 56.0, 35.7, 34.1. ESI-MS *m/z*: 493.25 $(M+H)^+$, calcd for $C_{26}H_{21}BrO_5$: 492.06.

5.1.11 Synthesis of compounds 34, **36 and 38**. Ethyl 2-bromoacetate, ethyl 4-bromobutanoate, or ethyl 5-bromopentanoate (0.56 mmol), followed by K_2CO_3 (77.5 mg, 1.13 mmol), was added at room temperature to a solution of **8a** (100 mg, 0.28 mmol) in acetone (20 mL). The reaction mixture was then refluxed for 8 h. The resulting mixture was filtered and the filter cake was washed with acetone (20 mL). The filtrate was concentrated under reduced pressure, the residue was dissolved in

MeOH and H_2O (20 mL, v/v 2:1), and 6N-HCl was added dropwise to the solution. The reaction mixture was stirred at room temperature for 3-5 h, quenched with saturated aqueous NH_4Cl solution (20 mL), and extracted with EtOAc (3 × 20 mL). The combined organic layers were washed with brine (50 mL), dried over $MgSO_4$, filtered, and concentrated under reduced pressure. The residue was purified by chromatography on silica gel to obtain the desired compounds **34**, **36**, and **38**.

5.1.11.1 (*E*)-Ethyl 2-{4-[3-(5-allyl-hydroxy-2-methoxyphenyl)acryloyl]phenoxy}acetate (34). Yellow solid, 56.32% yield. m.p: 166.7-168.9 °C. ^{1}H-NMR (500 MHz, acetone-d_6) δ (ppm): 8.03 (d, *J* = 8.0 Hz, 2H), 7.71 (d, *J* = 3.3 Hz, 1H), 7.52 (d, *J* = 15.7 Hz, 1H), 7.36 (s, 1H), 6.98 (d, *J* = 8.5 Hz, 2H), 6.49 (s, 1H), 5.90 (dd, *J* = 16.7, 6.5 Hz, 1H), 4.95 (s, 2H), 4.93 (dd, *J* = 17.1, 1.7 Hz, 1H), 4.87 (d, *J* = 8.9 Hz, 1H), 4.15-4.13 (m, 2H), 3.74 (s, 3H), 3.22 (d, *J* = 6.5 Hz, 2H), 1.72 (s, 3H) ^{13}C-NMR (125 MHz, acetone-d_6) δ (ppm): 189.6, 169.2, 163.9, 158.9, 140.7, 136.4, 130.9 ×2, 130.6, 130.5, 121.3, 116.0, 115.7 ×2, 114.8, 108.2, 107.3, 102.4, 65.3, 61.2, 56.1, 34.1, 14.1. ESI-MS *m/z*: 397.14 $(M+H)^+$, calcd for $C_{23}H_{24}O_6$: 396.16.

5.1.11.2 (*E*)-Ethyl4-{4-[3-(5-allyl-4-hydroxy-2-methoxyphenyl)acryloyl]phenoxy}butanoate (36). Yellow solid, 62.50% yield, m.p: 156.6-158.3 °C. ^{1}H NMR (500 MHz, acetone-d_6) δ (ppm): 8.91 (s, 1H), 7.96 (d, *J* = 2.5 Hz, 1H), 7.93 (d, *J* = 9.6 Hz, 2H), 7.56 (d, *J* = 15.6 Hz, 1H), 7.49 (s, 1H), 6.93 (d, *J* = 8.8 Hz, 2H), 6.48 (s, 1H), 5.90 (dd, *J* = 16.7, 6.5 Hz, 1H), 4.93 (dd, *J* = 17.1, 1.7 Hz, 1H), 4.87 (d, *J* = 8.9 Hz, 1H), 4.75-4.69 (m, 2H), 4.19-3.99 (m, 2H), 3.73 (s, 3H), 3.22 (d, *J* = 6.5 Hz, 2H), 1.95-1.88 (m, 4H), 1.12 (dd, *J* = 9.1, 5.1 Hz, 3H). ^{13}C-NMR (125 MHz, acetone-d_6) δ (ppm): 188.5, 168.9, 162.4, 159.9, 159.5, 139.8, 138.0, 133.3, 131.4, 133.2 ×2, 120.1, 119.3, 116.5, 115.3, 115.2 ×2, 99.8, 66.8, 61.6, 56.0, 34.1, 30.6, 14.4. ESI-MS *m/z*: 425.12 $(M+H)^+$, calcd for $C_{25}H_{28}O_6$: 424.19.

5.1.11.3 (*E*)-Ethyl 5-{4-[3-(5-allyl-4-hydroxy-2-methoxyphenyl)acryloyl]phenoxy}pentanoate (38). Yellow solid, 50.66% yield, m.p: 178.3-180.3 °C. ^{1}H NMR (500 MHz, acetone-d_6) δ (ppm): 8.89 (s, 1H), 7.97-7.91 (m, 3H), 7.56 (d, *J* = 15.6 Hz, 1H), 7.48 (s, 1H), 6.91 (d, *J* = 8.8 Hz, 2H), 6.47 (d, *J* = 19.5 Hz, 1H), 5.90 (dd, *J* = 16.7, 6.5 Hz, 1H), 4.93 (dd, *J* = 17.1, 1.7 Hz, 1H), 4.87 (d, *J* = 8.9 Hz, 1H), 3.96 (dt, *J* = 14.2, 6.5 Hz, 4H), 3.73 (s, 3H), 3.22 (d, *J* = 6.5 Hz, 2H), 2.25 (t, *J* = 7.2 Hz, 2H), 1.75 – 1.60 (m, 4H), 1.32 (s, 3H). ^{13}C-NMR (125 MHz, acetone-d_6) δ (ppm): 188.4, 173.4, 163.5, 159.9, 159.5, 139.5, 138.1 ×2, 132.5, 131.5, 131.3, 120.1, 119.3, 116.5, 115.3, 115.0 ×2, 99.8, 68.5, 60.5, 56.0, 34.2, 34.1, 22.3, 14.5 ×2. ESI-MS *m/z*: 439.15 $(M+H)^+$, calcd for $C_{26}H_{30}O_6$: 438.20.

5.1.12 Synthesis of compounds 35, **37 and 39.** NaOH (10%, 5 mL) was added dropwise to a solution of **34**, **36,** or **38** (0.3 mmol) in MeOH (10 mL), and the reaction mixture was stirred at room temperature for 3 h. The resulting mixture was quenched by water (20 mL) and acidified to pH = 2 with 6N-HCl. The mixture was extracted with EtOAc (3 × 20 mL). The combined organic layers were washed with brine (50 mL), dried over $MgSO_4$, filtered, and concentrated under reduced pressure. The residue was purified by chromatography on silica gel to obtain the target compounds **35**, **37**, and **39**.

5.1.12.1 (*E*)-2-{4-{3-{5-Allyl-2-methoxy-4-[(tetrahydro-*2H*-pyran-2-yl)oxy]phenyl}acryloyl} phenoxy}acetic acid (35). Yellow liquid, 60.3% yield. ^{1}H-NMR (500 MHz, acetone-d_6) δ (ppm): 8.87 (s, 1H), 7.96 (d, *J* = 2.7 Hz, 2H), 7.56 (d, *J* = 15.6 Hz, 1H), 7.49 (s, 1H), 6.93 (d, *J* = 8.8 Hz, 2H), 6.48 (s, 1H), 5.90 (dd, *J* = 16.7, 6.5 Hz, 1H), 4.93 (dd, *J* = 17.1, 1.7 Hz, 1H), 4.87 (d, *J* = 8.9 Hz, 1H), 4.71 (s, 2H), 3.76 (s, 3H), 3.71 (s, 2H), 3.22 (d, *J* = 6.5 Hz, 2H). ^{13}C-NMR (125 MHz, acetone-d_6) δ (ppm): 188.4, 169.9, 162.4, 159.9, 139.7, 138.0, 133.3, 131.4, 131.2 ×2, 120.1, 119.3, 115.5, 115.2 ×2, 99.8, 65.8, 61.6, 56.0, 34.1, 14.4. ESI-MS *m/z*: 352.94 $(M+H)^+$, calcd for $C_{21}H_{20}O_5$:

352.13.

5.1.12.2 (*E*)-4-{4-[3-(5-Allyl-4-hydroxy-2-methoxyphenyl)acryloyl]phenoxy}butanoic acid (37). Yellow liquid, 64.6% yield. ^{1}H-NMR (500 MHz, acetone-d_6) δ (ppm): 8.79 (s, 1H), 7.97-7.91 (m, 3H), 7.56 (d, *J* = 15.6 Hz, 1H), 7.48 (s, 1H), 6.90 (d, *J* = 8.8 Hz, 2H), 6.47 (d, *J* = 19.5 Hz, 1H), 5.90 (dd, *J* = 16.7, 6.5 Hz, 1H), 4.93 (dd, *J* = 17.1, 1.7 Hz, 1H), 4.87 (d, *J* = 8.9 Hz, 1H), 3.96 (dt, *J* = 14.2, 6.5 Hz, 2H), 3.73 (s, 3H), 3.22 (d, *J* = 6.5 Hz, 2H), 2.25 (t, *J* = 7.2 Hz, 2H), 2.21 (t, *J* = 6.2 Hz, 2H), ^{13}C-NMR (125 MHz, acetone-d_6) δ (ppm): 188.4, 178.1, 165.3, 159.1, 15, 140.8, 139.5, 138.1 ×2, 131.3, 120.7, 119.1, 116.5, 115.3, 115.0 ×2, 99.8, 68.5, 60.5, 56.05, 34.2, 34.1, 22.3, 17.8. ESI-MS *m/z*: 397.42 $(M+H)^+$, calcd for: $C_{23}H_{24}O_6$: 396.16.

5.1.12.3 (*E*)-5-{4-[3-(5-Allyl-4-hydroxy-2-methoxyphenyl)acryloyl]phenoxy}pentanoic acid (39). Yellow liquid, 64.6% yield. ^{1}H NMR (500 MHz, acetone-d_6) δ (ppm): 8.79 (s, 1H), 7.97-7.91 (m, 3H), 7.56 (d, *J* = 15.6 Hz, 1H), 7.48 (s, 1H), 6.90 (d, *J* = 8.8 Hz, 2H), 6.47 (d, *J* = 19.5 Hz, 1H), 5.90 (dd, *J* = 16.7, 6.5 Hz, 1H), 4.93 (dd, *J* = 17.1, 1.7 Hz, 1H), 4.87 (d, *J* = 8.9 Hz, 1H), 3.96 (dt, *J* = 14.2, 6.5 Hz, 4H), 3.73 (s, 3H), 3.22 (d, *J* = 6.5 Hz, 2H), 2.25 (t, *J* = 7.2 Hz, 1H), 1.75-1.60 (m, 4H), ^{13}C-NMR (125 MHz, acetone-d_6) δ (ppm): 188.4, 178.1, 165.3, 159.1, 159.0, 140.8, 139.5, 138.1 ×2, 131.3, 120.7, 119.1, 116.5, 115.3, 115.0 ×2, 99.8, 68.5, 60.5, 56.0, 34.2, 34.1, 22.3, 17.8. ESI-MS *m/z*: 411.38 $(M+H)^+$, calcd for $C_{24}H_{26}O_6$: 410.17.

5.2 Cell culture

HepG2 cells were cultured in minimum essential medium alpha containing 10% fetal bovine serum, penicillin (100 U/mL), and streptomycin (0.1 mg/mL). The cells were maintained at 37 °C in an atmosphere with 5% CO_2, and the medium was changed twice a week. In order to establish a cellular model of insulin-resistance, the cells were treated with PA (0.15 mM) for 24 h. PA was

dissolved in 7% bovine serum albumin (BSA). Cells cultured in a medium containing 7% BSA were used as controls. HepG2 cells and insulin-resistant cells were seeded on 6-well plates, and pretreated for 1 h with PTP1B inhibitors at 5 or 10 μM. The cells were then incubated with or without PA for 24 h. Finally, the cells were harvested after being stimulated with 100 nM insulin.

The cells were washed twice with ice-cold PBS and lysed in radioimmunoprecipitation assay buffer containing phenylmethylsulfonyl fluoride, Na_3VO_4, aprotinin, leupeptin, and protein phosphatase inhibitor. The lysates were then centrifuged at 4 °C and 12000 rpm for 10 min. The supernatant was subject to Bradford and immunoblotting assays. Total proteins were separated using 10% sodium dodecyl sulfate-polyacrylamide gel electrophoresis, and then electrotransferred to polyvinylidene difluoride membranes. The membranes were blocked with 5% milk for 2 h at room temperature, and then incubated with primary antibodies overnight at 4 °C. The membranes were washed three times with Tris-buffered saline-Tween for 5 min each and incubated with horseradish peroxidase (HRP)-conjugated secondary antibodies for 1.5 h at room temperature. Finally, protein bands were visualized by Gel Imaging System using an electrochemical luminescence detection kit.

5.3 Animal model

The animal protocol was approved by the Animal Care and Use Committee of the Wenzhou Medical University (Approval documents: wydw2014-0001). Eight-week-old db/db mice were orally administered Compound **23** or a vehicle every day for 10 weeks. The mice were then sacrificed, and their serum samples were collected to detect AKP, ALT, and TCH by using standard assay kits (Jiancheng Bioengineering Institute, Nanjin). Liver tissues were immersed in liquid nitrogen and stored at -80 °C. Histomorphological examination was conducted using hematoxylin and eosin (H&E) staining. The tissue samples were then lysed and subjected to immunoblotting for P-IRS-1 (CST, USA).

5.4 PTP1B and related PTPs biological assay

Recombinant human PTP1B was purchased from BIOMOL International LP (Plymouth Meeting,

PA). For the inhibition assay, a sample (3 μL in DMSO) was added to a reaction mixture containing enzyme (2 μL), reaction buffer [10 μL, 50 mM citrate (pH 6.0), 0.1 M NaCl, 1 mM EDTA, and 1 mM dithiothreitol], water (35 μL), and 4 mM *p*NPP (50 μL). The reaction mixture (100 μL) was incubated at 37 °C for 30 min and then quenched with 10 μL of 10 N NaOH. The hydrolysis of *p*NPP was determined by measuring the absorbance at 405 nm.

5.5 Histopathological examination

For light microscopic examination, the livers of the dissected animals were cleared from adhering tissues, fixed in Bouin's fixative for 24 h, and then processed for paraffin embedding. After routine processing, paraffin sections of the liver tissues were cut into 5-6 cm-thick slices and stained with H&E. The H&E stained slides were studied under an optical light microscope and the architecture of hepatocytes, central vein, and sinusoids, as well as the abundance of pyknotic nuclei in the liver tissue, were observed.

5.6 The pharmacokinetics study

Male Sprague–Dawley (SD) rats weighing 200 ± 20 g (Shanghai Laboratory Animal Center of the Chinese Academy of Sciences, Shanghai, China) were used in the pharmacokinetics study. The rats were kept under standard laboratory conditions at Laboratory Animal Research Center of Wenzhou Medical University and provided with food and tap water *ad libitum*. Diet was prohibited for 12 h before experiment. Blood samples were collected from the tail vein at 0.083, 0.25, 0.5, 1, 2, 4, 6, 9, 12, and 24 h after intragastric or intravenous injection. The samples were centrifuged at 3000 × *g* for 10 min, and the supernatants were removed and stored at -20 °C until analysis. Serum samples were analyzed by UPLC-coupled tandem mass spectrometry (UPLC-MC/MC) using an Agilent 1290 UPLC and 6420 series Triple-Quadrupole Tandem Mass Spectrometer equipped with an electrospray ionization (ESI) source.

5.7 Molecular docking

The crystal structure of the protein PTP1B was obtained from the Protein Data Bank (PDB ID: 1Q1M). The water molecules and original ligand were manually removed by using the PyMol software.[29] This docking task was performed to predict the binding position of **23** in PTP1B by using the software Autodock (version 4.2.6).[30] In the beginning, _ligand4.py and _recptor4.py scripts were prepared from AutoDockTools 1.5.6 that was used to prepare the initial files, including additional charges and hydrogen atoms. A grid box of 60 × 60 × 60 with a spacing of 0.375 Å was positioned to enclose the entire binding site. The Lamarckian genetic hypothesis was adopted to search the best binding positions. The specific docking settings were as follows. The trials were of 100 dockings, involving 300 individuals per population with a crossover rate of 0.8, and the local search rate was set at 0.06. Other parameters were set as default during the docking assay.

5.8 Molecular dynamics simulations

The best docking structure of Compound **23** in a complex with PTP1B was used as the initial structure for the conventional molecular dynamics (MD) simulation. The partial charge of Compound **23** was optimized by using the restrained electrostatic potential fitting procedure at Level HF 6-31G in the Gaussian 09 package.[31] Molecular mechanics parameters from ff14SB and general AMBER force field were assigned to the protein and ligand, respectively, by applying the LEaP module of the AMBER 16 software suite.[32] This complex was solvated in a rectangular box of transferable intermolecular potential with 3 points (TIP3P) water molecules with an extending range of 10 Å from the protein. Further, this system was neutralized by adding an appropriate amount of sodium ions. To avoid steric clashes, two-step minimization was performed prior to the MD productive simulation. Since the beginning, water molecules were minimized through 2500 steps of steepest descent, followed by 2500 steps of conjugate gradient steps. The same minimization protocol was then applied to the entire system. The TIP3P box was then generally heated at a constant volume from 0 to 300 K over a coupling time of 100ps with position restraints. Subsequently, the entire system was equilibrated over 100 ps at a constant pressure of 1 bar to accommodate solvent density. Another 100 ps equilibration was performed to allow pressure

relaxation without constraints. Finally, a 50 ns MD simulation was conducted. During the running process, periodic boundary conditions were turned on, and the Particle Mesh Ewald approach was used to deal with long-range electrostatic interactions, whereas a cutoff of 10 Å was defined for van der Waals interactions.[33] All hydrogen atoms were constrained using the SHAKE algorithm and the time step was set to 2 fs.[34] The trajectory frames were saved every 10 ps for subsequent analyses.

5.9 Analysis of MD trajectories and calculation of binding free energy

The MM/GBSA method is an Amber module widely used to calculate the binding free energy of biomolecular interactions and to decompose energy contributions into individual residues.[35,36] According to this system, snapshots were extracted from the 8 ns before conformational transition and the last 10 ns MD trajectory for average calculation, using the following equations:

$$\Delta G_{bind} = \Delta G_{complex} - (\Delta G_{receptor} + \Delta G_{ligand}) \quad (1)$$

$$\Delta G_{bind} = \Delta H - T\Delta S \approx \Delta E_{MM} + \Delta G_{sol} - T\Delta S \quad (2)$$

$$\Delta E_{MM} = \Delta E_{internal} + \Delta E_{vdW} + \Delta E_{elec} \quad (3)$$

$$\Delta G_{sol} = \Delta G_{GB} + \Delta G_{SA} \quad (4)$$

In eq. (3), ΔE_{MM} can be decomposed into three terms: intramolecular energy ($\Delta E_{internal}$ including bonds, angles, and dihedral energies), van der Waals energy (ΔE_{vdW}), and electrostatic energy (ΔE_{elec}). ΔG_{GB} and ΔG_{SA} are the polar and nonpolar components of solvation free energy, respectively. $T\Delta S$ represents entropy change upon ligand binding.

5.10 Statistical analysis

Data are expressed as mean ± standard error of the mean (SEM). The Student's *t*-test was employed to analyze differences between sets of data. Statistical analyses were performed using the GraphPad Pro software (GraphPad, San Diego, CA). P values less than 0.05 ($P < 0.05$) were considered statistically significant. All experiments were repeated at least three times.

Acknowledgements

This research was supported by the National Natural Science Foundation of China (21502144, 81773579), as well as the Basic Research Program, through the National Research Foundation (NRF) of Korea, funded by the Ministry of Education (Grant No. 2012R1A1A2006613). We gratefully acknowledge the Gwangju branch of the Korea Basic Science Institute (KBSI) for performing the NMR and ESI-MS experiments.

References

[1] Ardito F, Giuliani M, Perrone D, Troiano G, Lo Muzio L. The crucial role of protein phosphorylation in cell signaling and its use as targeted therapy (Review). *Int J Mol Med*. 2017;40:271-280.

[2] Belfiore A, Malaguarnera R, Vella V, Lawrence MC, Sciacca L, Frasca F, Morrione A, Vigneri R. Insulin receptor isoforms in physiology and disease: an updated view. *Endocr Rev.* 2017;38:379-431.

[3] Zhang S, Zhang ZY. PTP1B as a drug target: recent developments in PTP1B inhibitor discovery. *Drug Discov Today* 2007;12:373-381.

[4] Elchebly M, Payette P, Michaliszyn E, Cromlish W, Collins S, Loy AL, Normandin D, Cheng A, Himms-Hagen J, Chan CC, Ramachandran C, Gresser MJ, Tremblay ML, Kennedy BP. Increased insulin sensitivity and obesity resistance in mice lacking the protein tyrosine phosphatase-1B gene. *Science* 1999;283:1544-1548.

[5] Tsou RC, Rak KS, Zimmer DJ, Bence KK. Improved metabolic phenotype of hypothalamic PTP1B-deficiency is dependent upon the leptin receptor. *Mol Metab*. 2014;3:301-312 .

[6] Zinker BA, Rondinone CM, Trevillyan JM, Gum RJ, Clampit JE, Waring JF, Xie N, Wilcox D, Jacobson P, Frost L, Kroeger PE, Reilly RM, Koterski S, Opgenorth TJ, Ulrich RG, Crosby S, Butler M, Murray SF, McKay RA, Bhanot S, Monia BP, Jirousek MR. PTP1B antisense oligonucleotide lowers PTP1B protein, normalizes blood glucose, and improves insulin sensitivity in diabetic mice. *Proc Natl Acad Sci U S A* 2002;99:11357-11362.

[7] Bialy L, Waldmann H. Inhibitors of protein tyrosine phosphatases: Next-generation drugs? *Angew Chem Int Edit.* 2005;44:3814-3339.

[8] Tamrakar AK, Maurya CK, Rai AK. PTP1B inhibitors for type 2 diabetes treatment: a patent review (2011-2014). *Expert Opin Ther Pat*. 2014;24:1101-1115.

[9] Li X, Wang L, Shi D. The design strategy of selective PTP1B inhibitors over TCPTP. *Bioorg Med Chem*. 2016;24:3343-3352.

[10] Yarchoan M, Arnold SE. Repurposing diabetes drugs for brain insulin resistance in alzheimer disease. *Diabetes* 2014;63:2253-2261.

[11] Jin T, Yu H, Huang XF. Selective binding modes and allosteric inhibitory effects of lupane triterpenes on protein tyrosine phosphatase 1B. *Sci Rep*. 2016;6:20766.

[12] Smith AM, Maguire-Nguyen KK, Rando TA, Zasloff MA, Strange KB, Yin VP. The protein tyrosine phosphatase 1B inhibitor MSI-1436 stimulates regeneration of heart and multiple other tissues. *NPJ Regen Med.* 2017;2:4.

[13] Yoon G, Do Jung Y, Cheon SH. Cytotoxic allyl retrochalcone from the roots of Glycyrrhiza inflata. *Chem Pharm Bull.* 2005;53:694-695.

[14] Nagai H, He JX, Tani T, Akao T. Antispasmodic activity of licochalcone A, a species-specific ingredient of Glycyrrhiza inflata roots. *J Pharm Pharmacol.* 2007;59:1421-1426.

[15] Tanifuji S, Aizu-Yokota E, Funakoshi-Tago M, Sonoda Y, Inoue H, Kasahara T. Licochalcones suppress degranulation by decreasing the intracellular Ca2+ level and tyrosine phosphorylation of ERK in RBL-2H3 cells. *Int Immunopharmacol.* 2010;10:769-776.

[16] Yoon G, Lee W, Kim SN, Cheon SH. Inhibitory effect of chalcones and their derivatives from Glycyrrhiza inflata on protein tyrosine phosphatase 1B. *Bioorg Med Chem Lett.* 2009;19:5155-5157.

[17] Liu Z, Yoon G, Cheon SH. An enantioselective total synthesis of (S)-(-)-licochalcone E: determination of the absolute configuration. *Tetrahedron* 2010;66:3165-3172.

[18] Uddin Z, Song YH, Ullah M, Li Z, Kim JY, Park KH. Isolation and characterization of protein tyrosine phosphatase 1B (PTP1B) inhibitory polyphenolic compounds from dodonaea viscosa

and their kinetic analysis. *Front Chem.* 2018;6:40.

[19] Liu Z, Tang L, Zou P, Zhang Y, Wang Z, Fang Q, Jiang L, Chen G, Xu Z, Zhang H, Liang G. Synthesis and biological evaluation of allylated and prenylated mono-carbonyl analogs of curcumin as anti-inflammatory agents. *Eur J Med Chem.* 2014;74:671-682.

[20] Chen G, Liu Z, Zhang Y, Shan X, Jiang L, Zhao Y, He W, Feng Z, Yang S, Liang G. Synthesis and anti-inflammatory evaluation of novel benzimidazole and imidazopyridine derivatives. *ACS Med Chem Lett.* 2013;4:69-74.

[21] Consonni V, Todeschini R, Pavan M, Gramatica P. Structure/response correlations and similarity/diversity analysis by GETAWAY descriptors. 2. Application of the novel 3D molecular descriptors to QSAR/QSPR studies. *J Chem Inf Comp Sci.* 2002;42:693-705.

[22] Duchowicz PR, Castro EA, Fernandez FM, Gonzalez MP. A new search algorithm for QSPR/QSAR theories: Normal boiling points of some organic molecules. *Chem Phys Lett.* 2005;412:376-80.

[23] Alberca LN, Sbaraglini ML, Balcazar D, Fraccaroli L, Carrillo C, Medeiros A, Benitez D, Comini M, Talevi A. Discovery of novel polyamine analogs with anti-protozoal activity by computer guided drug repositioning. *J Comput Aided Mol Des.* 2016;30:305-321.

[24] Cheng ZY, Tseng Y, White MF. Insulin signaling meets mitochondria in metabolism. *Trends Endocrin Met.* 2010;21:589-598.

[25] Haeusler RA, McGraw TE, Accili D. Biochemical and cellular properties of insulin receptor signalling. *Nat Rev Mol Cell Bio.* 2018;19:31-44.

[26] Puius YA, Zhao Y, Sullivan M, Lawrence DS, Almo SC, Zhang ZY. Identification of a second aryl phosphate-binding site in protein-tyrosine phosphatase 1B: a paradigm for inhibitor design. *Proc Natl Acad Sci U S A* 1997;94:13420-13425.

[27] Whittier SK, Hengge AC, Loria JP. Conformational motions regulate phosphoryl transfer in related protein tyrosine phosphatases. *Science* 2013;341:899-903.

[28] Jia Z, Barford D, Flint AJ, Tonks NK. Structural basis for phosphotyrosine peptide recognition by protein tyrosine phosphatase 1B. *Science* 1995;268:1754-8.

[29] Alexander N, Woetzel N, Meiler J. bcl::Cluster : A method for clustering biological molecules coupled with visualization in the Pymol Molecular Graphics System. *IEEE Int Conf Comput Adv Bio Med Sci.* 2011;2011:13-8.

[30] Morris GM, Huey R, Lindstrom W, Sanner MF, Belew RK, Goodsell DS, Olson AJ. AutoDock4 and AutoDockTools4: Automated docking with selective receptor flexibility. *J Comput Chem.* 2009;30:2785-91.

[31] Wojcik J, Ratuszna A, Peszke J, Wrzalik R. Theoretical reproduction of the Q-band absorption spectrum of free-base chlorin. *J Chem Phys.* 2015;142:034302.

[32] Maier JA, Martinez C, Kasavajhala K, Wickstrom L, Hauser KE, Simmerling C. ff14SB: improving the accuracy of protein side chain and backbone parameters from ff99SB. *J Chem Theory Comput.* 2015;11:3696-3713.

[33] Sagui C, Darden TA. Molecular dynamics simulations of biomolecules: long-range electrostatic effects. *Annu Rev Biophys Biomol Struct.* 1999;28:155-179.

[34] Krautler V, Van Gunsteren WF, Hunenberger PH. A fast SHAKE: Algorithm to solve distance constraint equations for small molecules in molecular dynamics simulations. *J Comput Chem.* 2001;22:501-508.

[35] Gohlke H, Case DA. Converging free energy estimates: MM-PB(GB)SA studies on the protein-protein complex Ras-Raf. *J Comput Chem.* 2004;25:238-250.

[36] Kollman PA, Massova I, Reyes C, Kuhn B, Huo S, Chong L, Lee M, Lee T, Duan Y, Wang W, Donini O, Cieplak P, Srinivasan J, Case DA, Cheatham TE 3rd. Calculating structures and free energies of complex molecules: Combining molecular mechanics and continuum models. *Acc Chem Res.* 2000;33:889-897.

Graphical Abstract

Synthesis, biological evaluation, and molecular docking study of novel allyl-retrochalcones as a new class of protein tyrosine phosphatase 1B inhibitors

Yunjie Zhao [1,2 #], Yongkai Cao [3,#], Huizhen Chen [4,#], Fei Zhuang [1], Chao Wu [1], Goo Yoon [5], Weiwei Zhu [1], Ying Su1, Suqing Zheng [1], Zhiguo Liu [1,*], Seung Hoon Cheon [2,*]

[1] *Chemical Biology Research Center at School of Pharmaceutical Sciences, Wenzhou Medical University, 1210 University Town, Wenzhou, Zhejiang 325035, China.*
[2] *College of Pharmacy and Research Institute of Drug Development, Chonnam National University, 77 Yongbong-Ro, Buk-Gu, Gwangju 61186, Korea.*
[3] *Guangdong Key Laboratory for Genome Stability & Disease Prevention, School of Pharmaceutical Science, Shenzhen University Health Science Center, Shenzhen, 518060, China.*
[4] *College of Chemistry & Materials Engineering, Wenzhou University, Wenzhou, Zhejiang 325035, China.*
[5] *College of Pharmacy and Natural Medicine Research Institute, Mokpo National University, Jeonnam 58554, Korea.*